Leptophobic Z' bosons in the secluded UMSSM

Mariana Frank,[1,*] Yaşar Hiçyılmaz,[2,3,†] Stefano Moretti,[2,‡] and Özer Özdal[1,2,§]

[1]*Department of Physics, Concordia University, 7141 Sherbrooke St. West, Montreal, Quebec, Canada H4B 1R6*

[2]*School of Physics & Astronomy, University of Southampton, Highfield, Southampton SO17 1BJ, UK*

[3]*Department of Physics, Balıkesir University, TR10145 Balıkesir, Turkey*

(Received 18 July 2020; accepted 16 November 2020; published 21 December 2020)

We perform a comprehensive analysis of the secluded supersymmetric $U(1)'$ model, consistent with present experimental constraints. We find that, in this model, the additional Z' gauge boson can be leptophobic without resorting to gauge kinetic mixing and consequently, also d-quark-phobic, thus lowering the LHC bounds on its mass. The model can accommodate very light singlinos as DM candidates, consistent with present day cosmological and collider constraints. Light charginos and neutralinos are responsible for muon anomalous magnetic predictions within 1σ of the measured experimental value. Finally, we look at the possibility that a lighter Z', expected to decay mainly into chargino pairs and followed by the decay into lepton pairs, could be observed at 27 TeV.

DOI: 10.1103/PhysRevD.102.115025

I. INTRODUCTION

With the discovery of the Higgs boson, the last piece of the Standard Model (SM) construction was fit into place. Furthermore, almost all SM predictions have been confirmed by experimental results, even precision tests involving higher order perturbative electroweak (EW) and quantum chromodynamics (QCD) effects. However, as it stands, the SM cannot be the final theory, and the quest for physics beyond the SM (BSM) is very much alive. Among the many proposed BSM scenarios, supersymmetry (SUSY) appears to be one of the most popular ones, since it provides elegant solutions to the SM drawbacks, such as the stabilization of the EW scale under radiative corrections and an explanation for the baryon asymmetry of the Universe and for the presence of dark matter (DM) in it. However, the minimal version of SUSY, the minimal supersymmetric SM (MSSM), provides no explanation for the μ problem [1–4]. The μ parameter, the so-called higgsino mass term, is expected to be at the SUSY-breaking scale but, for successful EW symmetry breaking, its value should be at the scale of the latter. Adding a $U(1)'$ gauge symmetry to the MSSM, one solves this problem by replacing the μ parameter of the MSSM with an effective one, generated dynamically by the vacuum expectation value (VEV) of the singlet Higgs field responsible for breaking $U(1)'$. Furthermore, the additional $U(1)'$ symmetry is able to generate neutrino masses by allowing right-handed neutrinos into the superpotential and can account for either Majorana- [5] or Dirac-type neutrinos [6].

Normally, it is expected that both EW and $U(1)'$ symmetry breaking are achieved through soft-breaking parameters, which would imply that the mass of the gauge boson associated with $U(1)'$, a Z', would be of the same order as the EW scale [7–9]. This conflicts with experimental measurements at the Large Hadron Collider (LHC) [10], though, which impose a lower bound on the Z' mass, from the Drell-Yan (DY) channel, i.e., dilepton hadroproduction, of $\mathcal{O}(4)$ TeV or more. The most natural solution to this inconsistency is that the VEV of the singlet Higgs field is large compared to the EW scale, $\mathcal{O}(1–10)$ TeV, pushing the SUSY scale very high and rendering it mostly unobservable at the present LHC. Alternatively, it was observed that fine-tuning the kinetic mixing between the two $U(1)$ groups could yield Z' bosons, which do not decay directly into lepton pairs [11]. Corresponding Z' gauge boson masses are then limited by its dijet decays, whose bounds are much weaker in comparisons to DY ones [12]. Various aspects of the additional gauge boson and its phenomenological implications have been also studied within non-SUSY and SUSY frameworks [13–23].

An alternative is represented by a $U(1)'$ model where the SUSY-breaking scale and Z' mass are disjoint: The former is close to the EW scale, while a large value for the latter can be generated by the VEVs of additional Higgs fields

*mariana.frank@concordia.ca
†y.hicyilmaz@soton.ac.uk
‡s.moretti@soton.ac.uk
§ozer.ozdal@soton.ac.uk

(S_1, S_2, S_3, so-called secluded singlets), which are charged under the $U(1)'$ group but couple weakly to the SM fields [24]. This BSM scenario is known as the secluded $U(1)'$ model, a realization of the generic class of $U(1)'$-extended MSSMs (UMSSMs). It allows for both explicit and spontaneous charge parity (CP) symmetry breaking and is able to account for baryogenesis [25]. Differences between this UMSSM scenario and the MSSM would likely reveal themselves in the nature of DM; as in, the extended scenario several additional singlinos as well as sneutrinos could be viable candidates for it [26].

In a nutshell, the secluded $U(1)'$ model extends the MSSM by an additional Abelian group, to $SU(3)_c \otimes SU(2)_L \otimes U(1)_Y \otimes U(1)'$, and by four Higgs singlets (three in addition to the one needed to break $U(1)'$ to ensure a $Z' - Z$ mass hierarchy [24]). Exotics with Yukawa couplings to a singlet Higgs field must be introduced to ensure the theory is anomaly free. However, despite the presence of these couplings, one can assume their masses to be at the grand unified theory (GUT) scale and thus neglect them in TeV scale phenomenology.[1] (Note, however, that they have been studied extensively in [27].) Previous studies of this secluded $U(1)'$ model exist, but since they are older [26,28], none of them are consistent with present experimental data on the discovered Higgs boson mass and signal strengths or with Z' gauge boson mass bounds. In this work, we revisit this BSM scenario in detail, with particular interest in addressing the unresolved problems of UMSSMs, by providing light Z' masses yet compatible with current bounds, an acceptable $(g-2)_\mu$ value, and DM relic density, plus the viable existence of light SUSY particles, altogether providing one with new distinguishing signals of this BSM realization in LHC experiments.

In showing all this, we shall prove first that, in such a $U(1)'$ secluded model, leptophobia can be achieved easily and without gauge kinetic mixing between the Z and Z' so that a light Z' gauge boson can survive all experimental constraints in the presence of finite width effects. Furthermore, we shall show that this BSM scenario can predict corrections to $(g-2)_\mu$ within 1σ of the experimentally observed value. Finally, we will also find that, in our UMSSM realization, the lightest SUSY particle (LSP) for a large region of its parameter space is a singlino consistent with all DM constraints accompanied by very light charginos and neutralinos, with masses of $\mathcal{O}(100)$ GeV, and is in turn consistent with collider limits, into which a Z' can then decay yielding sizable signals at the LHC.

Our work is organized as follows. In the next section, Sec. II, we provide a description of the secluded $U(1)'$ model, with particular emphasis on the gauge and neutralino sectors, i.e., where differences with respect to the MSSM will manifest themselves. We describe the implementation of this BSM scenario, including the free parameters and the constraints imposed on these in Sec. III. Then, we explain the implications emerging from a wide scan of its parameter space for Z' physics at colliders in Sec. IV and onto the DM candidate in relic density and direct detection experiments in Sec. V. Furthermore, in presence of all such constraints on the mass and coupling spectrum of the model, we analyze the consequences for the muon anomalous magnetic moment in Sec. VI. We further study the possibility of observing a light Z' boson via chargino and neutralino decays at the high-luminosity LHC (HL-LHC) and high-energy LHC (HE-LHC) in Sec. VII. Finally, in Sec. VIII, we summarize our findings and draw our conclusions.

II. THE SECLUDED $U(1)'$ MODEL

In this section, we review the secluded $U(1)'$, known also as the secluded UMSSM. In addition to the MSSM superfields, the model has three right-handed neutrino superfields $\hat{N}_i^c$ and four scalar singlets $\hat{S}$, $\hat{S}_1$, $\hat{S}_2$, and $\hat{S}_3$. An anomaly-free model with an additional $U(1)'$ gauge group can be obtained by embedding it into an E_6 GUT. Breaking E_6 yields a combination of two additional $U(1)'$ gauge groups, denoted by $U(1)_\chi$ and $U(1)_\psi$, whose charges mix with angle θ_{E_6},

$$Q' = Q_\chi \cos\theta_{E_6} + Q_\psi \sin\theta_{E_6}, \tag{2.1}$$

where the orthogonal combination of $U(1)_\chi$ and $U(1)_\psi$ is assumed to be very heavy and decoupled.

Three **27** representations of E_6 are needed to provide three families of SM fermions, one pair of Higgs doublets, extra SM singlets, plus exotics. In the usual connection established between the breaking of $E6$ and the SM, a pair of $\mathbf{27} + \mathbf{27}^\star$ (sometimes referred to as $\mathbf{27}_L + \mathbf{27}_L^\star$) are introduced, in addition to the three **27** representations, to ensure gauge unification without anomalies [29]. These fundamental representations are connected, through the breaking $E6 \to SO(10) \to SU(5)$, to states in the SM. The breaking of the fundamental representation **27** of $E6$ yields $\mathbf{16} + \mathbf{10} + \mathbf{1}$ representations of $SO(10)$, with further decay into $SU(5)$ multiplets proceeding as $\mathbf{16} \to 10(u, d, u^c, e^+) + 5^\star(d^c, \nu, e^-) + 1(\bar{N})$, $\mathbf{10} \to 5(D, H_u) + 5^\star(D^c, H_d)$, and $\mathbf{1} \to 1(S_L)$, where we have indicated in brackets the remaining particle states. In addition to the SM particles, there are two exotic $SU(2)_L$ singlet quarks of charge $\pm 1/3$ and the singlets S_L and $\bar{N}$, in the conventional $E6$ notation. In our model, S, S_1, S_2, S_3 correspond to, respectively, S_L, $S_L^\star$, $S_L^\star$, and $\bar{N}^\star$ from two partial pairs of $\mathbf{27} + \mathbf{27}^\star$. The two $\mathbf{27} + \mathbf{27}^\star$ representations include the extra S_L and $\bar{N}$ to cancel the $U(1)'$ anomalies [29,30].

The complete description of E_6 SUSY GUTs, including composition of the fundamental **27** representation, has appeared in [31,32]. The secluded model corresponds to $\theta_{E_6} = \arctan\frac{\sqrt{15}}{9} \sim 0.13\pi$ and a prescribed set of $U(1)'$

[1] Furthermore, their charges are such that they do not mix with ordinary matter.

charges. The model was shown to, in addition to generating the μ term dynamically, be anomaly free [7], solve the $Z - Z'$ mass hierarchy [24], and facilitate EW baryogenesis [33,34]. In our study, we modify the model by reassigning the $U(1)'$ charges to allow the model to be leptophobic. As such, we cannot rely on previous restrictions on the model and shall perform a complete analysis of its parameter space.

The superpotential in this model is described by

$$\begin{aligned} W = & Y_u^{ij}\hat{Q}_i\hat{H}_u\hat{u}_j^c - Y_d^{ij}\hat{Q}_i\hat{H}_d\hat{d}_j^c - Y_e^{ij}\hat{L}_i\hat{H}_d\hat{e}_j^c \\ & + Y_\nu^{ij}\hat{L}_i\hat{H}_u\hat{N}_i^c + \lambda\hat{H}_u\hat{H}_d\hat{S} + \frac{\kappa}{3}\hat{S}_1\hat{S}_2\hat{S}_3 \\ & + \sum_{n=1}^{n_\varphi} h_\varphi^i S\varphi_i\bar{\varphi}_j + \sum_{n=1}^{n_\Upsilon} h_\Upsilon^i S\Upsilon_i\bar{\Upsilon}_j, \end{aligned} \tag{2.2}$$

where the first line of Eq. (2.2) contains the usual terms of the MSSM, while the second line includes the additional interactions of right-handed neutrinos $\hat{N}_i^c$ (assumed to be Dirac fields here) and $\hat{H}_u$, as well as the singlet superfields $\hat{S}$, $\hat{S}_1$, $\hat{S}_2$, and $\hat{S}_3$, and where Υ_i and φ_i are n_φ, n_Υ, respectively, generations of exotic fermions, vectorlike with respect to the MSSM but chiral under $U(1)'$ symmetry. The $U(1)$ and $U(1)'$ charges associated with these exotics, as well as the number of families, are a direct consequence of the anomaly cancellation conditions, are listed in the Appendix (Sec. IX). The φ_i are color-singlet states, while the Υ_i are color-triplet states. Their charges depend on the choices of $U(1)'$ charges of the rest of the particles, and their mass is restricted by searches for exotic charged particles at the LHC. Although no specific searches for exactly this charge exist, fermions with exotic charges are expected to have masses larger than 1 TeV [35].[2] The effective μ term is generated dynamically as $\mu = \lambda\langle S\rangle$. The scalar potential includes the F term, given by

$$\begin{aligned} V_F = & \lambda^2(|H_u|^2|H_d|^2 + |S|^2|H_u|^2 + |S|^2|H_d|^2) \\ & + \kappa^2(|S_1|^2|S_2|^2 + |S_2|^2|S_3|^2 + |S_3|^2|S_1|^2), \end{aligned} \tag{2.3}$$

while the D-term scalar potential is

$$\begin{aligned} V_D = & \frac{g_1^2 + g_2^2}{8}(|H_d|^2 - |H_u|^2)^2 \\ & + \frac{1}{2}g'^2\left(Q_S|S|^2 + Q_{H_u}|H_u|^2 + Q_{H_d}|H_d|^2 \right. \\ & \left. + \sum_{i=1}^{3} Q_{S_i}|S_i|^2\right)^2, \end{aligned} \tag{2.4}$$

where g_1, g_2, and g' are the coupling constants for the $U(1)_Y$, $SU(2)_L$, and $U(1)'$ gauge groups, while Q_ϕ is the $U(1)'$ charge of the field ϕ. Finally, the potential includes the SUSY-breaking soft terms,

TABLE I. Superfield configuration in the secluded UMSSM.

SF	Spin 0	Spin $\frac{1}{2}$	Generations	$U(1)_Y \otimes SU(2)_L \otimes SU(3)_C \otimes U(1)'$
$\hat{q}$	$\tilde{q}$	q	3	$(\frac{1}{6}, \mathbf{2}, \mathbf{3}, Q_q)$
$\hat{l}$	$\tilde{l}$	l	3	$(-\frac{1}{2}, \mathbf{2}, \mathbf{1}, Q_\ell)$
$\hat{H}_d$	H_d	$\tilde{H}_d$	1	$(-\frac{1}{2}, \mathbf{2}, \mathbf{1}, Q_{H_d})$
$\hat{H}_u$	H_u	$\tilde{H}_u$	1	$(\frac{1}{2}, \mathbf{2}, \mathbf{1}, Q_{H_u})$
$\hat{d}$	$\tilde{d}_R^*$	d_R^*	3	$(\frac{1}{3}, \mathbf{1}, \bar{\mathbf{3}}, Q_d$
$\hat{u}$	$\tilde{u}_R^*$	u_R^*	3	$(-\frac{2}{3}, \mathbf{1}, \bar{\mathbf{3}}, Q_u)$
$\hat{e}$	$\tilde{e}_R^*$	e_R^*	3	$(1, \mathbf{1}, \mathbf{1}, Q_e)$
$\hat{v}_R$	$\tilde{\nu}_R^*$	ν_R^*	3	$(0, \mathbf{1}, \mathbf{1}, Q_\nu)$
$\hat{S}$	S	$\tilde{S}$	1	$(0, \mathbf{1}, \mathbf{1}, Q_s)$
$\hat{S}_1$	S_1	$\tilde{S}_1$	1	$(0, \mathbf{1}, \mathbf{1}, Q_{s_1})$
$\hat{S}_2$	S_2	$\tilde{S}_2$	1	$(0, \mathbf{1}, \mathbf{1}, Q_{s_2})$
$\hat{S}_3$	S_3	$\tilde{S}_3$	1	$(0, \mathbf{1}, \mathbf{1}, Q_{s_3})$

$$\begin{aligned} V_{\text{soft}} = & m_{H_u}^2|H_u|^2 + m_{H_d}^2|H_d|^2 + m_S^2|S|^2 + \sum_{i=1}^{3} m_{S_i}^2|S_i|^2 \\ & - (A_\lambda\lambda S H_u H_d + A_\kappa\kappa S_1 S_2 S_3 + \text{H.c.}) \\ & + (m_{SS_1}^2 S S_1 + m_{SS_2}^2 S S_2 + m_{S_1S_2}^2 S_1^\dagger S_2 + \text{H.c.}). \end{aligned} \tag{2.5}$$

In Table I, we give the complete list of the fields in the model, together with their spin, number of generations, and charge assignments under the extended gauge group. The secluded $U(1)'$ charge assignments and anomaly cancellation conditions allow for some freedom in the choice of the $U(1)'$ charges, absent in other $U(1)'$ models. In general, the $U(1)'$ change assignments can be chosen as follows:

$$\begin{aligned} & Q_Q = \alpha, \qquad Q_{H_u} = \beta, \qquad Q_S = \gamma, \\ & Q_\ell = -3\alpha + \frac{\gamma}{3}, \qquad Q_{H_d} = -\beta - \gamma, \\ & Q_u = -\alpha - \beta, \qquad Q_d = -Q_Q - Q_{H_d} = -\alpha + \beta + \gamma, \\ & Q_e = -Q_\ell - Q_{H_d} = 3\alpha + \beta + \frac{2\gamma}{3}, \\ & Q_N = -Q_\ell - Q_{H_u} = 3\alpha - \beta - \frac{\gamma}{3}, \qquad Q_{S_1} = Q_{S_3} = \delta, \\ & Q_{S_2} = -2Q_{S_1} = -2Q_{S_3} = -2\delta. \end{aligned} \tag{2.6}$$

Here, $Q_{H_d} = 0$ dictates $\gamma = -\beta$. From the conditions above, we can choose, for simplicity, $Q_e = Q_\ell$. The leptophobic condition $Q_\ell = Q_e = 0$ requires $\alpha = -\frac{\beta}{9}$ so that the leptophobia condition can be achieved without resorting to kinetic mixing between the two $U(1)$ groups.[3] Thus, Eq. (2.6) can be rewritten in terms of α and δ only as

[2] These appear naturally and have been discussed in the context of E_6 gauge groups [36].

[3] This is unlike models where the $U(1)'$ charges are derived from the mixing of, e.g., θ_{E_6} angles [37].

$$
\begin{aligned}
&Q_Q = \alpha, \qquad Q_{H_u} = -9\alpha, \qquad Q_S = 9\alpha,\\
&Q_\ell = 0, \qquad Q_{H_d} = 0, \qquad Q_u = 8\alpha, \qquad Q_d = -\alpha,\\
&Q_e = 0, \qquad Q_N = 9\alpha, \qquad Q_{S_1} = Q_{S_3} = \delta,\\
&Q_{S_2} = -2Q_{S_1} = -2Q_{S_3} = -2\delta. \qquad (2.7)
\end{aligned}
$$

After the spontaneous breaking of the extended gauge symmetry group down to electromagnetism (EM), the $W^{\pm}, Z$ and Z' bosons acquire masses, while the photon remains massless. At tree level, the squared masses of the Z and Z' bosons are given by

$$
\begin{aligned}
M_Z^2 &= \frac{g_1^2 + g_2^2}{2}(\langle H_u^0\rangle^2 + \langle H_d^0\rangle^2),\\
M_{Z'}^2 &= g'^2\Big(Q_S\langle S\rangle^2 + Q_{H_u}\langle H_u^0\rangle^2 + Q_{H_d}\langle H_d^0\rangle^2\\
&\quad + \sum_{i=1}^{3} Q_{S_i}\langle S_i\rangle^2\Big), \qquad (2.8)
\end{aligned}
$$

where $H_d^0 \equiv \frac{v_d}{\sqrt{2}}$ and $H_u^0 \equiv \frac{v_u}{\sqrt{2}}$ stand for the neutral components of the down-type and up-type Higgs fields H_d and H_u.

While the chargino sector is unaltered, the neutralino sector of the secluded $U(1)'$ model includes five additional fermion fields: the $U(1)'$ gauge fermion $\tilde{Z}'$ and four singlinos $\tilde{S}$, $\tilde{S}_1$, $\tilde{S}_2$, $\tilde{S}_3$, in total, nine neutralino states $\tilde{\chi}_i^0$ $(i = 1, \ldots, 9)$ [24]:

$$
\tilde{\chi}_i^0 = \sum_a \mathcal{N}_{ia}^0 \tilde{G}_a, \qquad (2.9)
$$

where the mixing matrix $\mathcal{N}_{ia}^0$ connects the gauge-basis neutral fermion states to the physical-basis neutralinos $\tilde{\chi}_i^0$. The neutralino masses $M_{\tilde{\chi}_i^0}$ are obtained through the diagonalization $\mathcal{N}^0\mathcal{M}\mathcal{N}^{0T} = \mathrm{Diag}\{M_{\tilde{\chi}_1^0}, \ldots, M_{\tilde{\chi}_9^0}\}$. The 9×9 neutral fermion mass matrix is

$$
\mathcal{M} = \begin{pmatrix}
M_{\tilde{Z}} & 0 & -M_{\tilde{Z}\tilde{H}_d} & M_{\tilde{Z}\tilde{H}_u} & 0 & M_{\tilde{Z}\tilde{Z}'} & 0 & 0 & 0\\
0 & M_{\tilde{W}} & M_{\tilde{W}\tilde{H}_d} & -M_{\tilde{W}\tilde{H}_u} & 0 & 0 & 0 & 0 & 0\\
-M_{\tilde{Z}\tilde{H}_d} & M_{\tilde{W}\tilde{H}_d} & 0 & -\mu & -\mu_{H_u} & \mu'_{H_d} & 0 & 0 & 0\\
M_{\tilde{Z}\tilde{H}_u} & -M_{\tilde{W}\tilde{H}_u} & -\mu & 0 & -\mu_{H_d} & \mu'_{H_u} & 0 & 0 & 0\\
0 & 0 & -\mu_{H_u} & -\mu_{H_d} & 0 & \mu'_S & 0 & 0 & 0\\
M_{\tilde{Z}\tilde{Z}'} & 0 & \mu'_{H_d} & \mu'_{H_u} & \mu'_S & M_{\tilde{Z}'} & \mu'_{S_1} & \mu'_{S_2} & \mu'_{S_3}\\
0 & 0 & 0 & 0 & 0 & \mu'_{S_1} & 0 & -\frac{\kappa v_3}{3\sqrt{2}} & -\frac{\kappa v_2}{3\sqrt{2}}\\
0 & 0 & 0 & 0 & 0 & \mu'_{S_2} & -\frac{\kappa v_3}{3\sqrt{2}} & 0 & -\frac{\kappa v_1}{3\sqrt{2}}\\
0 & 0 & 0 & 0 & 0 & \mu'_{S_3} & -\frac{\kappa v_2}{3\sqrt{2}} & -\frac{\kappa v_1}{3\sqrt{2}} & 0
\end{pmatrix}, \qquad (2.10)
$$

where the lightest eigenvalue is the DM candidate. In the neutralino mass matrix, the mass mixing terms are defined in terms of $\tan\beta = \frac{v_d}{v_u}$, $\langle S\rangle = \frac{v_S}{\sqrt{2}}$ and $\langle S_i\rangle = \frac{v_i}{\sqrt{2}}$ $(i = 1, 2, 3)$ as

$$
\begin{aligned}
&M_{\tilde{Z}\tilde{H}_d} = M_Z \sin\theta_W \cos\beta, \quad M_{\tilde{Z}\tilde{H}_u} = M_Z \sin\theta_W \sin\beta,\\
&M_{\tilde{W}\tilde{H}_d} = M_Z \cos\theta_W \cos\beta, \quad M_{\tilde{W}\tilde{H}_u} = M_Z \cos\theta_W \sin\beta, \qquad (2.11)
\end{aligned}
$$

where μ_i, μ'_j stand for the effective couplings in each sector, given in terms of h_s or g', the coupling constant of $U(1)'$, as

$$
\begin{aligned}
&\mu_{H_d} = h_s\frac{v_d}{\sqrt{2}}, \quad \mu_{H_u} = h_s\frac{v_u}{\sqrt{2}}, \quad \mu'_{H_d} = g'Q_{H_d}v_d,\\
&\mu'_{H_u} = g'Q_{H_u}v_u, \quad \mu'_S = g'Q_S v_S, \quad \mu'_{S_i} = g'Q_{S_i}v_i. \qquad (2.12)
\end{aligned}
$$

In our further analysis, we impose gauge coupling unification by setting $g_1 = g_2 = g' \approx g_3$ at the GUT scale.

III. COMPUTATIONAL SETUP

Following the development of the model as in Sec. II, to enable our analysis and impose constraints coming from experimental data, we implement the model within a computational framework. We have then made use of SARAH (version 4.13.0) [38–40] to generate CalcHep [41] model files and a UFO [42] version of the model [43] so that we could employ MicrOMEGAs (version 5.0.9) [44] for the computation of the predictions relevant for our dark matter study and SPheno (version 4.0.4) [45,46] package for spectrum analysis. Note that SARAH (version 4.13.0) includes all RGE corrections to model parameters to second order, and these are intrinsically dependent on our choice of $U(1)'$ charges. In this package, the weak scale values of the gauge and

Yukawa couplings present in secluded UMSSM are evolved to the unification scale $M_{\rm GUT}$ via the RGEs. After $M_{\rm GUT}$ is determined by the requirement of the gauge coupling unification (by setting $g_1 = g_2 = g' \approx g_3$) through their RGE evolutions, all the soft supersymmetry breaking (SSB) parameters, along with the gauge and Yukawa couplings, are evolved back to the weak scale with the boundary conditions given at $M_{\rm GUT}$.

In order to apply the LHC constraints on the properties of Z' bosons, we calculate the Z' production cross section at next-to-leading order (NLO) accuracy in QCD [47,48]. This relies on the joint use of FeynRules version 2.3.36 [49] and the included NLOCT package [50], as well as FeynArts [51], for the automatic generation of a UFO library [42] containing both tree-level and counterterm vertices necessary at NLO. This UFO model is then used by MG5a_MC@NLO (version 2.7.3) [52] for the numerical evaluation of the hard-scattering matrix elements, which are convoluted with the NLO set of NNPDF 3.1 parton distribution functions (PDF) [53]. Using the decay table provided by the SPheno package and assuming the narrow-width approximation, we compare our predictions with the ATLAS and CMS limits on Z' bosons in the dilepton [10] and dijet [12,54] modes in order to estimate the impact of supersymmetric decay channels in the secluded UMSSM.

We make use of HiggsBounds [55] to constrain the possibility of BSM Higgs bosons detection at colliders and HiggsSignals [56] to test the signal strengths of the SM-like Higgs state. During the numerical analysis performed in this work, we have used the PySLHA 3.2.4 package [57] to read the input values for the model parameters that we encode under the SLHA format [58] and to integrate the various employed programs into a single framework.

Using our interfacing and following the Metropolis-Hastings technique, we performed a random scan over the parameter space, illustrated in Table II, where we restrict ourselves only to universal boundary conditions. Here, m_0 denotes the spontaneous symmetry breaking (SSB) mass term for all the scalars, while $M_{1/2}$ stands for the SSB mass terms for the gauginos including the one associated with the $U(1)'$ gauge group. As before, $\tan\beta$ is the ratio of VEVs of the MSSM Higgs doublets, A_0 is the SSB trilinear scalar interacting term,[4] λ is the coupling associated with the interaction of the $\hat{H}_u$, $\hat{H}_d$, and $\hat{S}$ fields, while κ is the coupling of the interaction of the $\hat{S}_1$, $\hat{S}_2$, and $\hat{S}_3$ fields. Trilinear couplings for λ and κ are defined as $A_\lambda\lambda$ and $A_\kappa\kappa$, respectively, at the SUSY scale. Here, Y_ν^{ij} is the Yukawa coupling of the term $\hat{L}_i\hat{H}_u\hat{N}_i^c$, and we vary only the diagonal elements in the range of 1×10^{-8}–1×10^{-7} while setting the off-diagonal elements to zero.

TABLE II. Scanning range of parameter space of the secluded $U(1)'$ model.

Parameter	Scanned range	Parameter	Scanned range
m_0	[0., 3.] TeV	v_S	[0.97, 15.8] TeV
$M_{1/2}$	[0., 3.] TeV	v_1	[1.6, 15.] TeV
$\tan\beta$	[1., 55.]	v_2	[0.8, 11.2] TeV
A_0/m_0	$[-3., 3.]$	v_3	[1.6., 15.] TeV
λ	$[3.\times10^{-2}, 0.6]$	κ	[0.3, 2.65]
A_λ	[1.8, 7.5] TeV	A_κ	$[-8.3, -0.2]$ TeV
$Y_\nu^{ij},(i=j)$	$[1\times10^{-8}, 1\times10^{-7}]$	$Y_\nu^{ij},(i\neq j)$	0.

The desired distribution here is to designed to generate a collection of secluded UMSSM solutions consistent with all constraints along with the relic density constraint and muon $g-2$ within 2σ.

We followed [59] where a simple method for analyzing the impact of precision EW data above and below the Z peak on flavor-conserving heavy new physics is implemented. There, the corrections to all leptonic data can be converted into oblique corrections to the vector boson propagators and condensed into seven parameters. Numerical fits for the new physics parameters are included, and the method is applied to generic Z' gauge bosons highlighting parameter combinations most strongly constrained. The authors report the 99% confidence level (C.L.) isocontours of bounds on $M_{Z'}/g'$ for a set of Z''s. Their constraints depend only on the leptonic and Higgs $U(1)'$ charges, Q_{H_u}, Q_{H_d}, Q_ℓ, Q_e, and the assumption that their arbitrary overall normalization is fixed, $Q_H^2 + Q_\ell^2 + Q_e^2 = 2$. Given that we fix $Q_\ell = Q_e = Q_{H_d} = 0$, the Z' gauge boson in our model cannot be considered as one of the given set of Z''s so that the bounds on $M_{Z'}/g'$ given by [59] are not applicable in a straightforward way. Therefore, we require a 2σ (i.e., 95% C.L.) agreement with EW precision observables, parametrized through the oblique parameters S, T, U [60–63]. The constraints from the latter are included by evaluating

$$\chi^2_{\rm STU} = X^T C^{-1} X, \tag{3.1}$$

with $X^T = (S-\hat{S}, T-\hat{T}, U-\hat{U})$. The observed parameters deviations are given by [64]

$$\hat{S} = 0.05, \qquad \hat{T} = 0.09, \qquad \hat{U} = 0.01, \tag{3.2}$$

where the unhatted quantities denote the model predictions. The covariance matrix is [64]

$$\mathbf{C}_{ij} = \begin{bmatrix} 0.0121 & 0.0129 & -0.0071 \\ 0.0129 & 0.0169 & -0.0119 \\ -0.0071 & -0.0119 & 0.0121 \end{bmatrix}. \tag{3.3}$$

We then require $\chi^2_{\rm STU} \leq 8.025$, corresponding to a maximal 2σ deviation, given the 3 degrees of freedom.

[4]Note that, while we scan A_0/m_0 between $[-3, 3]$, most of our solutions lie near $A_0 \approx 0$.

We also verified that the vertex corrections due to loops with supersymmetric particles are small. For the parameter space, which survives all constraints, $\mathrm{BR}(Z \to b\bar{b}) \in (0.1508 - 0.1510)$, which is consistent with the experimental requirement $\mathrm{BR}(Z \to b\bar{b}) = (15.12 \pm 0.005)\%$ [65].

IV. GAUGE BOSON MASS CONSTRAINTS

After imposing the constraints from the previous section, we turn our attention to gauge bosons. From the SSB of the $SU(2)_L \otimes U(1)_Y \otimes U(1)'$ symmetry, the gauge bosons Z and Z' mix to form physical mass eigenstates. The $Z - Z'$ mixing mass matrix is

$$\mathbf{M_Z^2} = \begin{pmatrix} M_{ZZ}^2 & M_{ZZ'}^2 \\ M_{ZZ'}^2 & M_{Z'Z'}^2 \end{pmatrix}. \tag{4.1}$$

As the mixing between the Z and Z' bosons is very small, to a good approximation, these are good physical states, with masses given in Eq. (2.8). Following the methodology described in the previous section, we scan the parameter space imposing constraints on SUSY particles, rare B-meson decays, and oblique parameters so that the SM Z gauge boson properties are consistent with experimental data, as indicated in Table III. In the following, we analyze the properties of the gauge sector for all scenarios accepted in our scanning procedure. In Fig. 1, we depict the relations between the parameters $M_{Z'}$, g'_{SUSY}, Q_Q, the ratio of $M_{Z'}/g'_{\mathrm{SUSY}}$, and χ^2_{STU}. Here, g'_{SUSY} is the coupling constant for the $U(1)'$ group at the SUSY-breaking scale. The color bar of the upper panels shows the χ^2_{STU} values for solutions with $\chi^2_{\mathrm{STU}} \leq 8.025$, while the color bar of the left bottom panel represents the gauge coupling g'_{SUSY}. According to the top left panel of Fig. 1, the ratio $M_{Z'}/g'_{\mathrm{SUSY}}$ can be as low as 2.2 TeV when the charge Q_Q is small (i.e., $[1. - 3.] \times 10^{-2}$), while the bound on $M_{Z'}/g'_{\mathrm{SUSY}}$ tends to increase up to 8 TeV for larger Q_Q values (i.e., 1×10^{-1}). Further, the top right and bottom left panels of Fig. 1 show that light Z' solutions consistent with the constraints given in Table III can be found to lie around 1.5 TeV. For heavier Z' masses, the range for the ratio $M_{Z'}/g'_{\mathrm{SUSY}}$ opens up to a larger interval. As seen from the bottom panels of the figure, the lowest bound on the ratio $M_{Z'}/g'_{\mathrm{SUSY}}$ can be fulfilled at 2117 GeV when $M_{Z'} = 1388$ GeV, the corresponding gauge coupling being $g'_{\mathrm{SUSY}} \simeq 0.66$, $Q_Q = 1.11 \times 10^{-2}$, and $\chi^2_{\mathrm{STU}} = 2.64$. The lowest bound on $M_{Z'}/g'_{\mathrm{SUSY}}$ increases drastically, up to 15.7 TeV, when g'_{SUSY} has its minimum value 0.25, $M_{Z'} = 3940$ GeV, and $\chi^2_{\mathrm{STU}} = 6.01$.

The modules created by SARAH for SPheno calculate the full one-loop and partially two-loop-corrected mass spectrum. While the experimental value for the Higgs mass is very precise, SARAH and SPheno maintains the uncertainty estimate around 2–3 GeV for sparticle masses [40]. It was shown that the sparticle spectrum can shift the Higgs boson mass by 1–2 GeV [70–74].

For each solution with Higgs boson mass between 122–128 GeV, we make use of HiggsBounds, which takes the Higgs sector predictions for each solution as input and then uses the values of production cross sections and decays from Higgs searches at LEP, the Tevatron, and the LHC to determine if each parameter point has been excluded, at 95% C.L. We accept all solutions with a ratio (k_0) less than 1 where k_0 is defined as $k_0 = O_{\mathrm{model}}/O_{\mathrm{obs}}$, for O a relevant observable, for the process with highest statistical sensitivity.

Moreover, we also make use of HiggsSignals, which is an additional package in HiggsBounds and checks how good a solution reproduces the Higgs mass and rate measurements. It performs a statistical test of the Higgs sector predictions for the secluded UMSSM using measurements of Higgs boson signal rates and masses from the Tevatron and the LHC. To do this, we have applied peak-centered χ^2-squared method along with a box-shaped PDF with Gaussian tails for the SM-like Higgs mass uncertainty. Then, we assume only solutions with total χ^2 value less than 90, which is obtained by the peak-centered χ^2 method for the SM-like Higgs boson.

In the top left panel of Fig. 2, we present the comparison of $\sigma(pp \to Z') \times \mathrm{BR}(Z' \to \ell\ell)$ vs $M_{Z'}$, consistent with the ATLAS data of [10], scanning through the whole parameter space and displaying the values of $\mathrm{BR}(Z' \to \ell\ell)$ in different color codes. The experimental constraints are the same as in Fig. 1, except that we relax the χ^2_{STU} value since we want to plot the branching ratios (BR) also for light Z' solutions, which are excluded by the χ^2_{STU} bound. Since we fix $Q_\ell = Q_e = 0$, the Z' state does not couple to $\ell\ell$.

TABLE III. Current experimental and theoretical bounds used to determine consistent solutions in our scans.

Observable	Constraints	Ref.	Observable	Constraints	Ref.
m_{h_1}	[122, 128] GeV	[66]	$m_{\tilde{t}_1}$	$\geq$730 GeV	[65]
$m_{\tilde{g}}$	$>$1.75 TeV	[65]	$m_{\tilde{\chi}_1^\pm}$	$\geq$103.5 GeV	[65]
$m_{\tilde{\tau}_1}$	$\geq$105 GeV	[65]	$m_{\tilde{b}_1}$	$\geq$222 GeV	[65]
$m_{\tilde{q}}$	$\geq$1400 GeV	[65]	$m_{\tilde{\mu}_1}$	$>$94 GeV	[65]
$m_{\tilde{e}_1}$	$>$107 GeV	[65]	$\lvert\alpha_{ZZ'}\rvert$	$\mathcal{O}(10^{-3})$	[8]
χ^2_{STU}	$\leq$8.025	–	$\mathrm{BR}(B_s^0 \to \mu^+\mu^-)$	$[1.1, 6.4] \times 10^{-9}$	[67]
$\frac{\mathrm{BR}(B\to\tau\nu_\tau)}{\mathrm{BR_{SM}}(B\to\tau\nu_\tau)}$	[0.15, 2.41]	[68]	$\mathrm{BR}(B^0 \to X_s\gamma)$	$[2.99, 3.87] \times 10^{-4}$	[69]

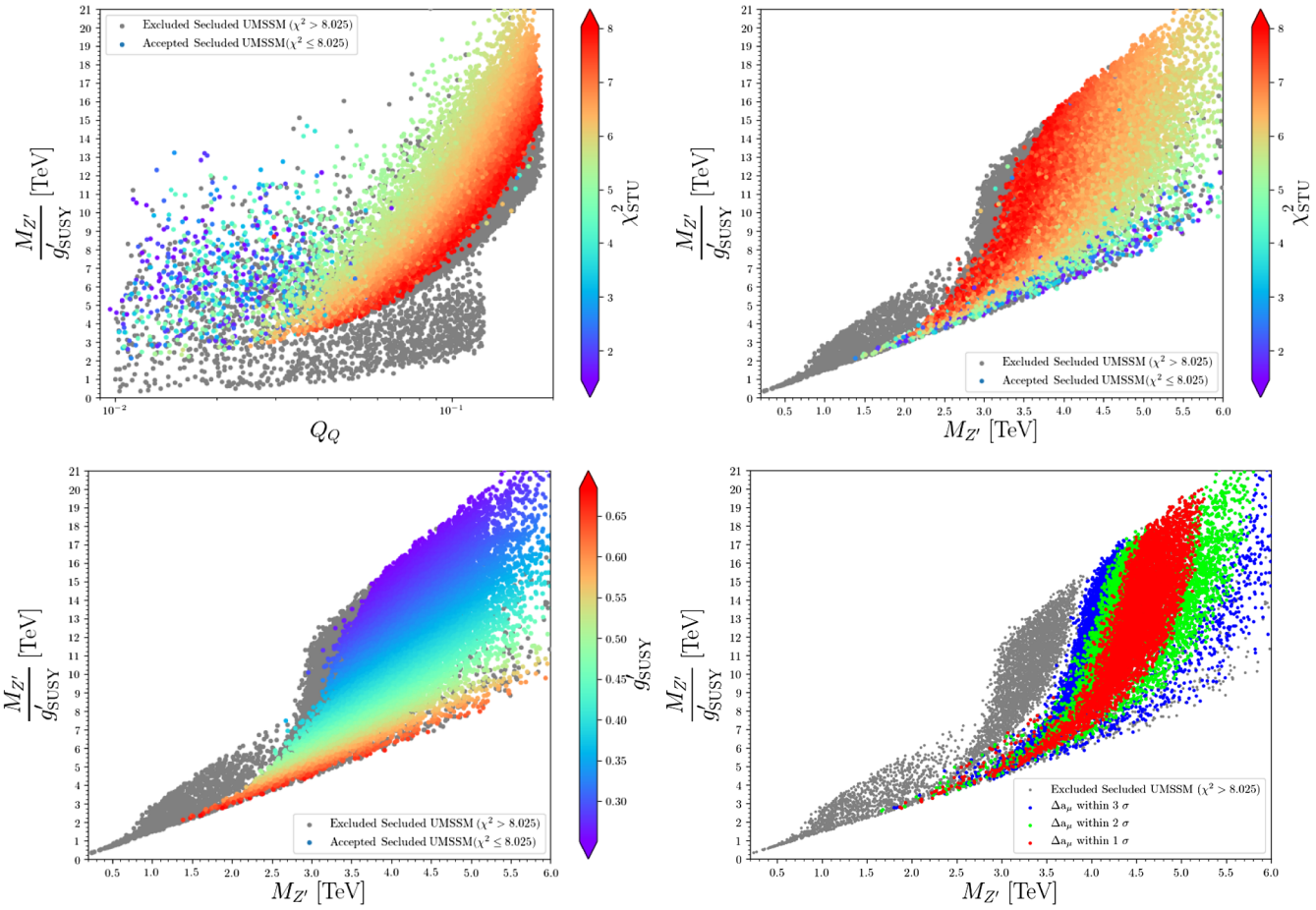

FIG. 1. The effect of oblique parameters and $(g-2)_\mu$ experimental bounds on the ratio $M_{Z'}/g'$.

However, the small mass mixing $Z - Z'$ still allows the Z' to decay into $\ell\ell$ states but only with BRs of 0.01% for $M_{Z'} \simeq 600$ GeV, while the BR decreases drastically for heavier Z' masses. The ATLAS observed limit on the fiducial cross section times BR ranges from 3.6 (13.1) fb at 250 GeV to about 0.014 (0.018) fb at 6 TeV for a zero (10%) relative width signal in the combined dilepton channel [10]. Therefore, our results imply a lower limit of ~700 GeV at the 95% C.L. on $M_{Z'}$ for the Z' boson in the combined dilepton channel. In the top right panel of Fig. 4, we compare the CMS high-mass dijet yield from Ref. [12] with our predictions for $\sigma(pp \to Z') \times \mathrm{BR}(Z' \to q\bar{q})$, obtained after scanning the secluded UMSSM parameters as described in Table II and imposing the constraints of Table III. For the sake of consistency with the experimental analysis, the $\sigma \times \mathrm{BR}$ rate is multiplied by an acceptance factor $A = 0.5$, and the fraction of $Z' \to t\bar{t}$ events is not included in the calculation.

These results are similar to those found in Z' models, which employ gauge kinetic mixing to achieve leptophobia. However, there are some differences. One is that, while in these other scenarios, the dijet BR of the Z' cannot be lowered below 36%, in the secluded UMSSM, it can be lowered to 5%. Another important aspect is that the model is also d-quark-phobic (the BR of Z' to d-type quarks is only about 1.4%). This is a direct consequence of different $U(1)'$ charge assignments, in particular of the fact that imposing leptophobia results in $Q_d = \alpha = \frac{Q_u}{8}$ [Eq. (2.7)]. Leptophobia and d-quark-phobia have thus further lowered the bound on the Z' mass by lowering its production cross section. Also, we benefit from new experimental acceptance ($A = 0.5$ with the new data at $\mathcal{L} = 137$ fb^{-1} [12], compared to $A = 0.6$ at $\mathcal{L} = 27$ fb^{-1} and 36 fb^{-1} [54]). From the top right panel of Fig. 2, one learns that the computed $\sigma \times \mathrm{BR}$ is always below the CMS exclusion limits [12,54] in the range 1.5 TeV $< M_{Z'} <$ 6 TeV at the 95% C.L., with the exception of a tiny region around $M_{Z'} \simeq 2.3$ TeV. One can, therefore, conclude that much lighter Z' bosons consistent with the constraints given in Table III could be allowed by data when leptophobic secluded UMSSM realizations, such as the one introduced in Sec. II, are considered. In the middle left panel, we check the ratio $\Gamma(Z')/M_{Z'}$ to assure that the narrow width approximation (NWA) can be used consistently, while in the middle right panel, we investigate the variation of the Z'

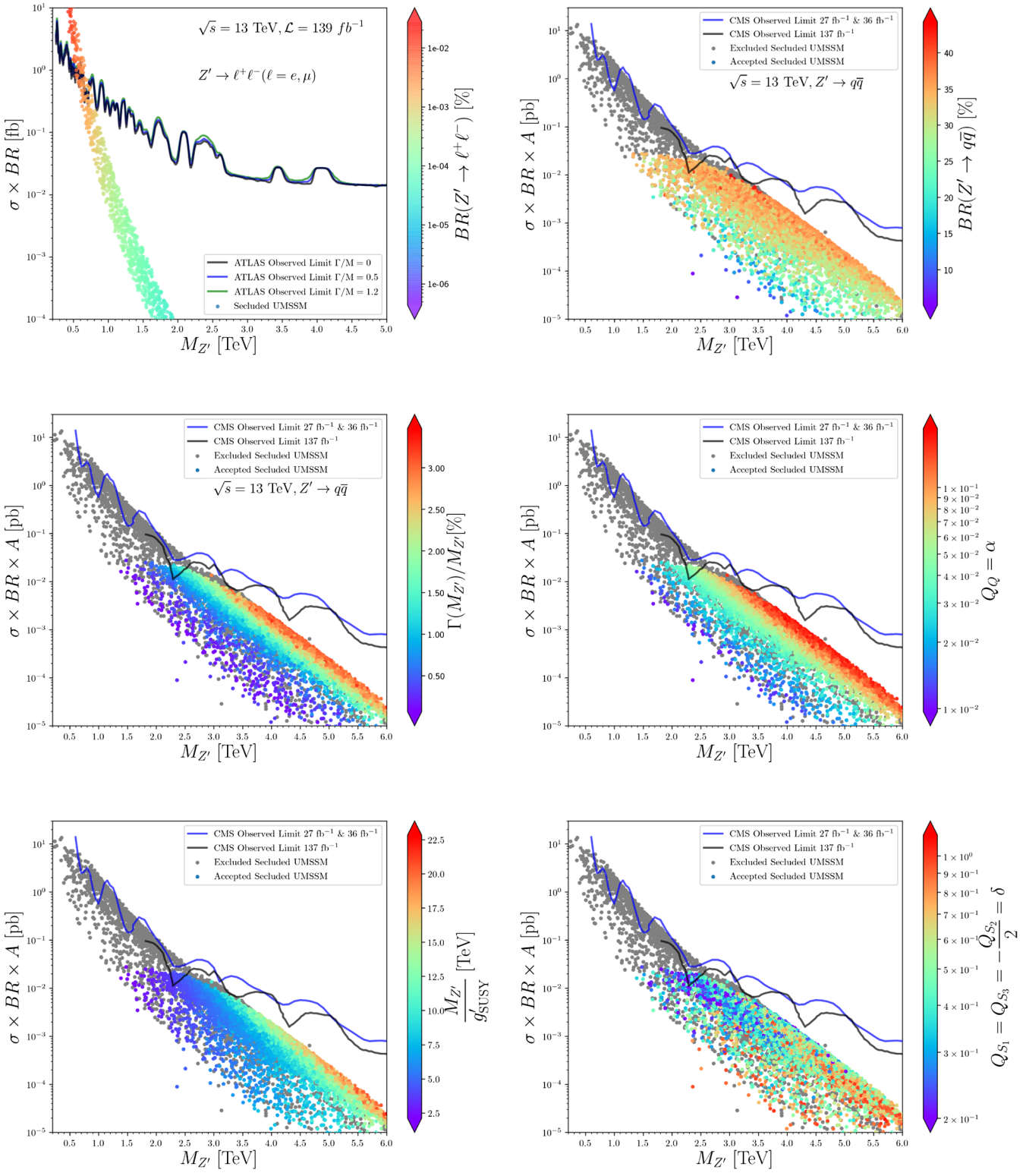

FIG. 2. Leptophobic Z' mass limits $Q_\ell = Q_e = 0$. We investigate the Z' production cross section multiplied by the dilepton and dijet BR (and by the acceptance $A = 0.5$ for the latter), respectively. We compare theoretical predictions of the secluded UMSSM to the bounds obtained by the ATLAS [10] and CMS [12,54] Collaborations.

mass limit with the Q_Q charge, $Q_Q = \alpha$, the free parameter for the matter fields in the secluded $U(1)'$ group. As seen from the color bar in the middle left panel, the Z' is quite narrow for the solutions found, while the color bar of the middle right panel indicates that also the α parameter should be quite small (less than $\alpha < 2 \times 10^{-1}$). Moreover,

one can see the correlation between α and $\Gamma(Z')/M_{Z'}$. When α is increased, the $\Gamma(Z')/M_{Z'}$ ratio also increases and approaches the CMS observed limits. As seen from the bottom left panel of Fig. 2, $M_{Z'}/g'$ ratios below ∼3 TeV require a decay width smaller than 1% and a Q_Q value smaller than $\sim 2 \times 10^{-2}$. Finally, the bottom right panel of Fig. 2 shows the relation between various Z' masses and the $U(1)'$ charges for the S_1, S_2, and S_3 secluded singlets, where we set $Q_{S_1} = Q_{S_3} = -Q_{S_2}/2 = \delta$ for simplicity. Solutions with lighter Z' masses necessitate smaller δ values, while δ values increase for heavier Z' masses. This relation can be understood via Eq. (2.8).

V. NEUTRALINO DARK MATTER

In this section, we analyze the model parameters, which survive cosmological bounds from the DM experiments. We investigate the constraints on the model arising from requiring the lightest neutralino to be a viable DM candidate, with properties compatible with current cosmological data.

In the MSSM, the neutral higgsinos (nearly mass degenerate with the higgsino-like charginos) could then play the role of the LSP. However, the relic density upper limit favors a neutralino with a large higgsino or wino component as the LSP. A pure higgsino LSP cannot saturate the relic density constraint unless its mass is ∼1 TeV [77]. Consequently, one needs the admixture of light binos and higgsinos to form a light DM candidate, as the minimal ingredient of a natural MSSM [78]. For DM lighter than about 100 GeV, in the MSSM, the chargino mass limit from the LEP experiments requires the DM to be bino dominated. Then, the weak interaction of the DM, together with a significant mass splitting of the DM from the other sparticles, typically leads to the overproduction of DM in the early universe [78]. As a result, only a small corner of the MSSM parameter space survives. A DM candidate lighter than about 30 GeV has been excluded in the MSSM [79]. In the NMSSM, instead, it would be possible for the singlino to be quite light but, there, correct relic density is obtained in the case when a small singlino mass results only from mixing with the neutral higgsinos [80].

Previous studies of $U(1)'$'s discussed light neutralino DM [81,82] before imposing limits from Higgs data and/or Z' mass and BR constraints and outside a leptophobic scenario. We revisit the light neutralino sector in our leptophobic scenario, while including all relevant constraints. First, we demand that the predicted relic density agrees within 20% (to conservatively allow for uncertainties on the predictions) with the recent Planck results, $\Omega_{\rm DM}h^2 = 0.12$ [75,76]. We calculate, for all points returned by our scanning procedure in Table II that are in addition compatible with current experimental bounds given in Table III, the associated DM relic density. We present our results in Fig. 3.

In all the subfigures, the relic density is plotted as a function of the mass of the lightest neutralino, denoted by $M_{\tilde{\chi}_1^0}$. As seen from the panels, solutions consistent with the relic density constraint emerge for almost all values of $M_{\tilde{\chi}_1^0}$ depending on the $\tilde{\chi}_1^0$ composition, which is given in the following basis: $(\tilde{B}', \tilde{B}, \tilde{W}, \tilde{H}_u, \tilde{H}_d, \tilde{S}, \tilde{S}_1, \tilde{S}_2, \tilde{S}_3)$. The color bar of the top left panel of Fig. 3 shows the $\tilde{S}$ content, as we are particularly interested in singlinos as non-MSSM LSP candidates. One can learn from this panel that the relic density observed by the Planck Collaboration can be accommodated by $\tilde{S}$-like $\tilde{\chi}_1^0$s lying roughly in the [25, 300] GeV window, a region largely disfavored for MSSM neutralinos where universal boundary conditions are applied at the GUT scale [78,85,86]. Once the lightest neutralino spectrum becomes heavier, the contribution of the combination of $\tilde{S}_1$, $\tilde{S}_2$, and $\tilde{S}_3$ singlets increases, so as to become dominant for $M_{\tilde{\chi}_1^0}$ heavier than 400 GeV, as seen from the upper right panel of Fig. 3. In the middle left panel, we focus on the combined contribution of all singlinos, that is, $\tilde{S}$, $\tilde{S}_1$, $\tilde{S}_2$, and $\tilde{S}_3$. As seen from the panel, singlinolike LSP solutions largely dominate the parameter space. The middle right panel shows the higgsinolike neutralino content. As observed from the panel, the relic density is at the scale of 10^{-3} for higgsinolike neutralino with $M_{\tilde{\chi}_1^0} \sim 100$ GeV, but it increases dramatically for heavier higgsinolike neutralino masses. As in the MSSM, the relic density observed by the Planck Collaboration can be accommodated by higgsinolike solutions at roughly ∼1 TeV [77]. Since TeV scale neutralino solutions are naturally less appealing from a collider point of view, and we want to pay particular attention to singlino LSP scenarios, we did not increase the scanned neutralino mass range beyond 1 TeV. Although potentially viable scenarios could be obtained for even heavier neutralinos (in particularly, for winos), for the purpose of this work, we ignore this regime throughout. The bottom left panel of Fig. 3 represents the bino composition of the lightest neutralino. Note that only solutions with bino contribution larger than 20% are represented in the panel. Although there are some bino dominated $\tilde{\chi}_1^0$ solutions in our spectrum, their corresponding relic density mostly tends to lie in the [10, 100] range. An important fact is that the lightest binolike solutions can be obtained near 300 GeV. Bino contributions start to decrease, yielding lower values of the relic density and giving a maximum 50% contribution, when the relic density constraint is satisfied and $M_{\tilde{\chi}_1^0} \sim 400$ GeV. The other ∼50% contributions to mostly binolike solutions consistent with the relic density constraint mainly come from higgsinos and winos, both of which contribute more significantly for heavier $\tilde{\chi}_1^0$ masses, up to roughly 850 GeV, where we can classify the DM as mixed neutralino states. We summarize the various lightest neutralino DM compositions in the bottom right panel of Fig. 3. As seen from this panel, bino dominated neutralino solutions

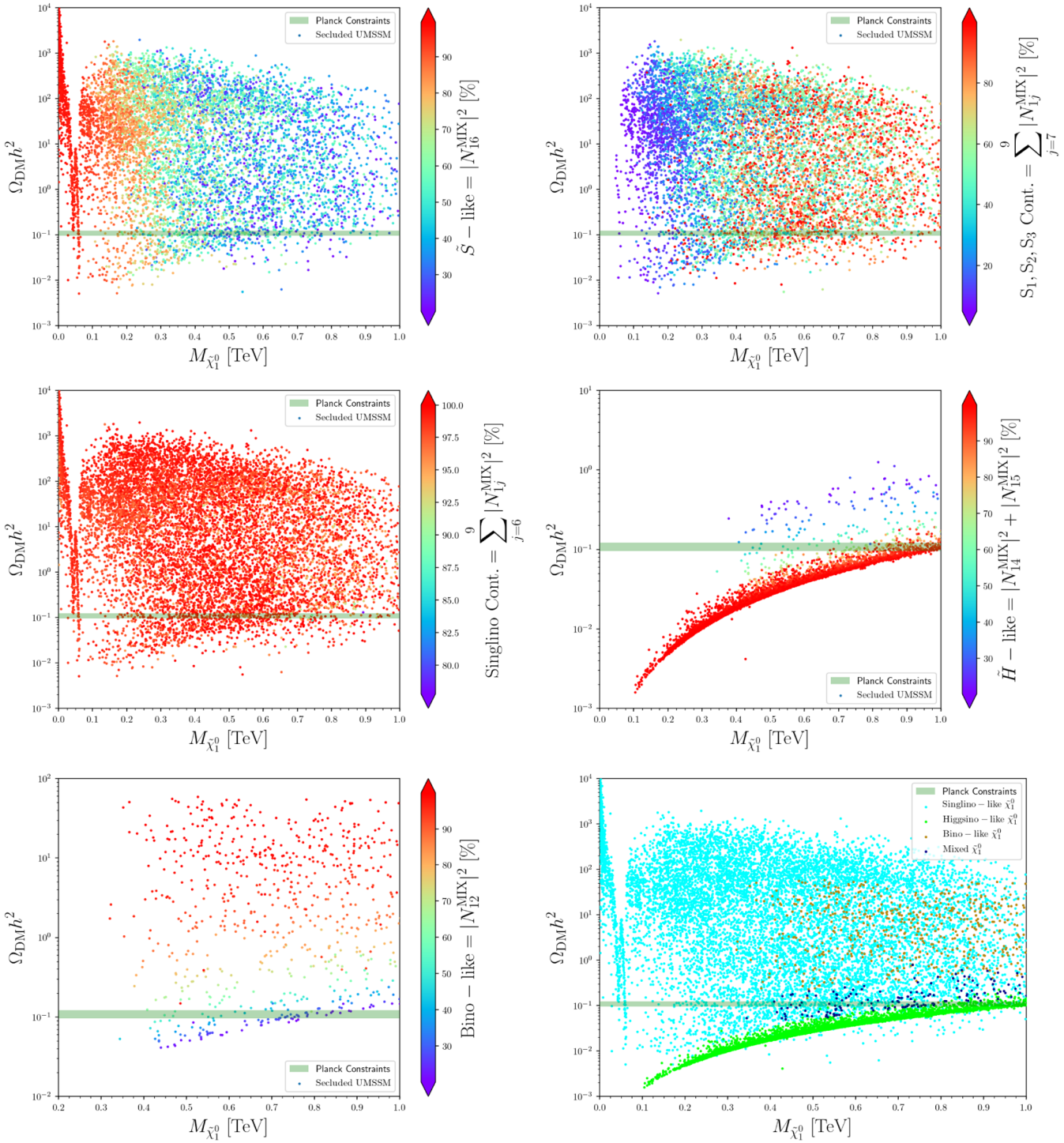

FIG. 3. Relic density predictions for secluded UMSSM scenarios satisfying all the constraints imposed during our scan and compatible with Z' bounds from the LHC, indicating the dependence on the mass of the lightest neutralino. In each panel of the figure, we analyze the composition of the LSP for different parameter regions. In the upper left panel, we represent by a color code the $\tilde{S}$-like contribution, while in the upper right panel, we show the combined contribution of $\tilde{S}_1$, $\tilde{S}_2$, and $\tilde{S}_3$. In the middle left panel, we show the total contribution from the singlinos while, in the middle right panel, we present the composition of MSSM-like higgsinos. The bottom left panel shows the contributions of the mostly bino solution while, in the bottom right panel, we indicate the parameter space populated by all the solutions. The horizontal green band in all panels indicates the measured value of the relic density, consistent at 2σ with the Planck experiment [75,76].

cannot be good candidates for DM since they do not satisfy the relic density constraints. Viable mixed (mostly bino and higgsino) neutralino DM solutions can be found with a mass lying in the 400–800 GeV range. When the spectrum is heavier, i.e., with a lightest neutralino $M_{\tilde{\chi}_1^0} \in [0.8\text{–}1.0]$ TeV, the relic density as observed by the Planck Collaboration can be accommodated by higgsino or singlino dominated solutions. It should be noted that $\tilde{B}'$ contributions are no more than 5% in the whole parameter space. Given that we mostly focus on small Q_Q values, this leads to small couplings with the gaugino $\tilde{B}'$ associated with the $U(1)'$ gauge group, so relatively small $\tilde{B}'$ contributions are expected.

Finally, we depict, in Fig. 4, the constraints coming from direct detection experiments. The top panels show the spin-independent cross section for the nucleon as a function of the mass of the lightest neutralino. Note that the results for spin-independent cross sections for the proton and neutron are almost the same. Therefore, we denoted it as $\sigma_{\mathrm{SI}}^{\mathrm{nucleon}}$ and normalized it to the present-day relic density. The top left plane shows how the spin-independent cross section for the nucleon depends on the composition of the lightest neutralino for solutions, which survive all the constraints given in Table III. Blue solutions in the top right panel refer to all solutions represented in the top left plane while all the other colors are subsets of blue and represent solutions consistent with the relic density constraint in addition to the ones in Table III. The black line indicates the limits from the Xenon 1T [87] with the region above the curve being excluded. In addition, the blue and red lines show the prospects for XENON nT and DARWIN [88] collaborations, respectively. As seen from the top left plane, almost all singlino solutions survive the results of the Xenon 1T experiment [87], while some portion of higgsino and bino dominated solutions are excluded. Another important feature is that all mixed neutralino solutions are strictly excluded by Xenon 1T. Once we compare our solutions consistent with the relic density bound to the

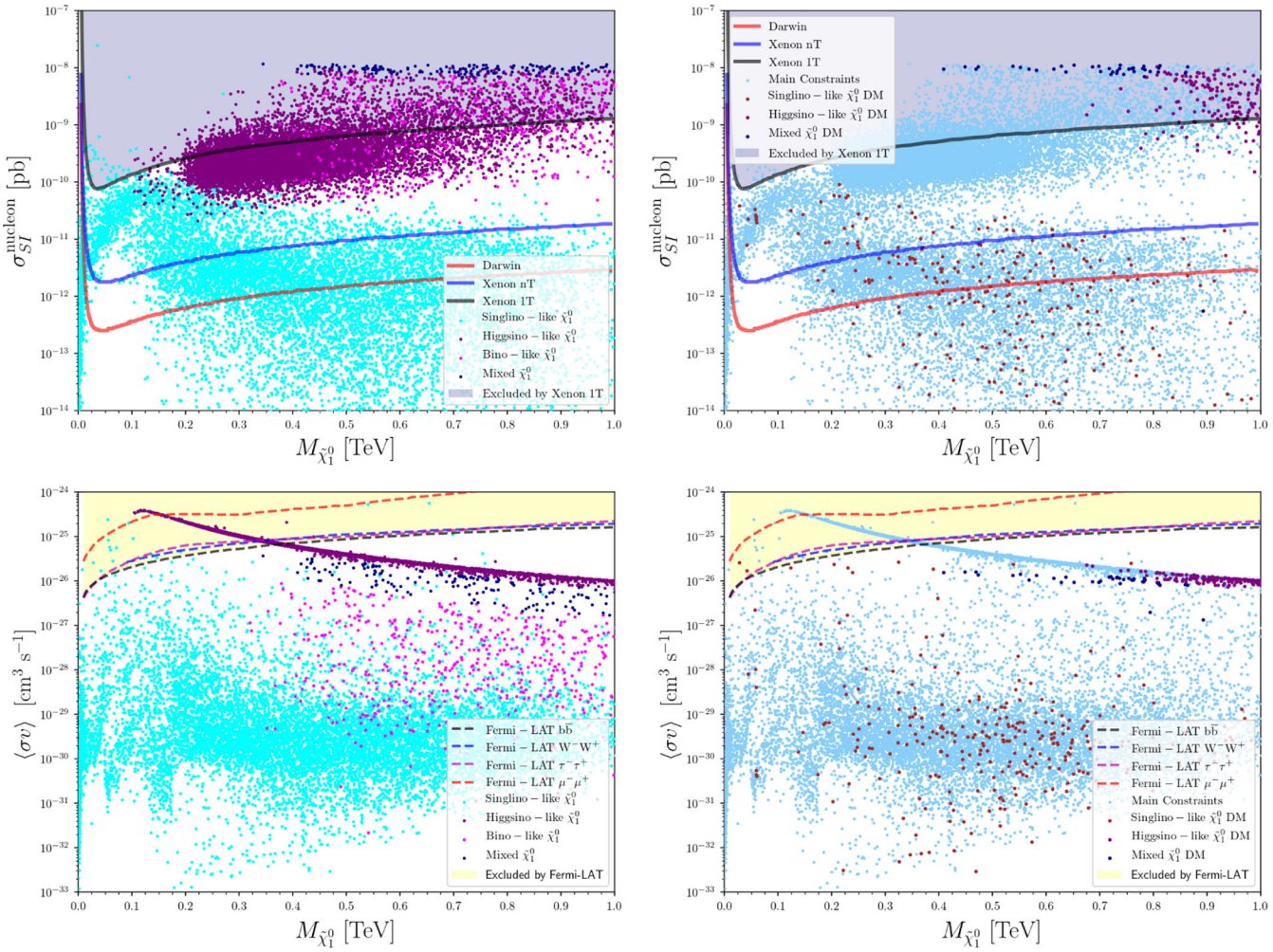

FIG. 4. DM direct and indirect detection constraints on the parameter space on the secluded UMSSM model. The top panels show the constraints from the spin-independent cross section for the nucleon, while the bottom panels show the corresponding annihilation cross sections.

result of Xenon 1T, a large fraction of higgsino dominated solutions consistent with the former are excluded by the latter as seen from the top right figure. In contrast, singlino DM solutions consistent with the relic density bound are always below the excluded region by Xenon 1T and can be probed by the next generation of DM experiments such as Xenon nT and Darwin.

While we have demonstrated that the singlino-type lightest neutralino could be a viable DM candidate from the point of view of the relic density and direct detection bounds, at the same time, it is important to verify that DM indirect detection bounds are also satisfied. In the bottom panels of Fig. 4, we present the value of the total DM annihilation cross section at zero velocity as a function of the lightest LSP neutralino mass for all scanned scenarios satisfying the Z' boson limits from the LHC. Configurations for which the relic density is found in agreement with Planck data are shown along with their higgsino, singlino, and mixed compositions in the bottom right panel, while any other setup returned by the scan is shown in light sky blue and tagged as "main constraints," referring to those given in Table III. In our predictions, we rescaled also the DM annihilation cross section to its present-day density. We compare our predictions to the latest bounds derived from the Fermi-LAT data [89,90]. We depict, as a yellow area, the parameter space region that is found out to be excluded. The bottom panel of Fig. 4 indicates that, unlike relic density and direct detection bounds, which impose strong constraints on the model parameters, indirect detection experiments are easily satisfied for a large portion of the parameter space. Most singlino DM scenarios naturally feature an annihilation cross section that is at least 3 or 4 orders of magnitude too small to leave any potentially visible signal in Fermi-LAT data. Therefore, singlino DM solutions are unaffected by current indirect detection limits and will potentially stay so for some time by virtue of their correspondingly small annihilation cross sections. In contrast, the annihilation cross sections of higgsino and mixed neutralino solutions are about 10^{-26} cm^3 s^{-1}; hence, they are more likely to be probed by Fermi-LAT when the precision of the annihilation cross section measurement will be improved.

In addition to the neutralino, in the secluded UMSSM, the sneutrino can be the LSP and thus a candidate for DM. Unfortunately, for most of the sneutrino LSP solutions, the relic density is overabundant compared to the requirements of the Planck Collaboration [75,76]. In addition, the spin-independent cross sections of all sneutrino LSP solutions are populated in the region excluded by XENON1T [87]. This is because, when the sneutrino is the LSP, it includes more $\tilde{\nu}_L$ components than $\tilde{\nu}_R$. Inevitably, then, the LSP sneutrino interacts more with $SU(2)_L$ doublets, and the spin-independent (SI) dark matter (DM)-nucleon cross section increases into the region excluded by XENON1T. Therefore, the LSP sneutrino is not a promising candidate in the secluded UMSSM.

VI. MUON ANOMALOUS MAGNETIC MOMENT

The measurement of the muon anomalous magnetic moment exhibits an intriguing discrepancy between the value found from the E821 experiment at BNL [91] and the value predicted by the SM. Adding uncertainties, the deviations amount to 3.5σ [65,92], while recent theory predictions for a_μ find values as large as 4.1σ,

$$\Delta a_\mu \equiv a_\mu^{\rm exp} - a_\mu^{\rm SM} = 268(63)(43) \times 10^{-11}.$$

Several models have been constructed and dedicated entirely to explain this discrepancy. Conversely, whether the discrepancy is real or not,[5] it has been used as a test of how well BSM scenarios perform.

In the secluded UMSSM, loop diagrams with additional neutralinos and sleptons as well as with (right) sneutrinos and charginos provide additional contributions to the $(g-2)_\mu$ observable. The parameter space is restricted by limits on slepton masses from LHC. While these are not as restrictive as gluino or squark mass limits, bounds on selectron and smuon masses are 550 GeV and 560 GeV, respectively [93,94], while staus are allowed to be as light as 390 GeV [95,96].

We present the results of our analysis in Fig. 5, where we show solutions consistent with the muon anomalous magnetic moment within 1σ of the experimental value. Here, we indicate the model solutions over the following planes: ($M_{\tilde{\chi}_1^\pm}$, $M_{\tilde{\chi}_1^0}$) (top left); ($M_{\tilde{\chi}_1^\pm}$, $M_{\tilde{\chi}_2^0}$) (top right); ($M_{\tilde{\chi}_1^\pm}$, $M_{\tilde{\chi}_3^0}$) (bottom left); and ($M_{\tilde{\nu}_1}$, $M_{\tilde{\tau}_1}$) (bottom right). When the lightest neutralino is singlino, the second and the third lightest ones are higgsinolike, rather light and almost degenerate in mass. The main contribution to the muon anomalous magnetic moment comes from these two heavier states as well as (albeit more marginally) from the lightest (right) sneutrino, and (through slepton-mixing) stau states, in the appropriate diagrammatic combinations. As seen from the figure, a large portion of the solution satisfies the Δa_μ bound within 1σ. The gray region below the black curve represents the parameter region ruled out by ATLAS searches [83,84], close to which, most solutions are found.

At the same time, the anomalous magnetic moment of the electron was also measured precisely to be [97] $a_e^{\rm exp} = 1.15965218076(28) \times 10^{-3}$, while calculations within the SM, considering QED contributions up to 10 loops, obtain $a_e^{\rm SM} = 1.159652181643(25)(23)(16)(763) \times 10^{-3}$ [98,99], yielding a difference close to 2.4σ between experiment and theory for Δa_e and of the opposite sign than the corresponding one for the muon:

[5]Leading order hadronic vacuum polarization contributions represent the main limitation of theoretical calculations of nonperturbative low-energy QCD behavior.

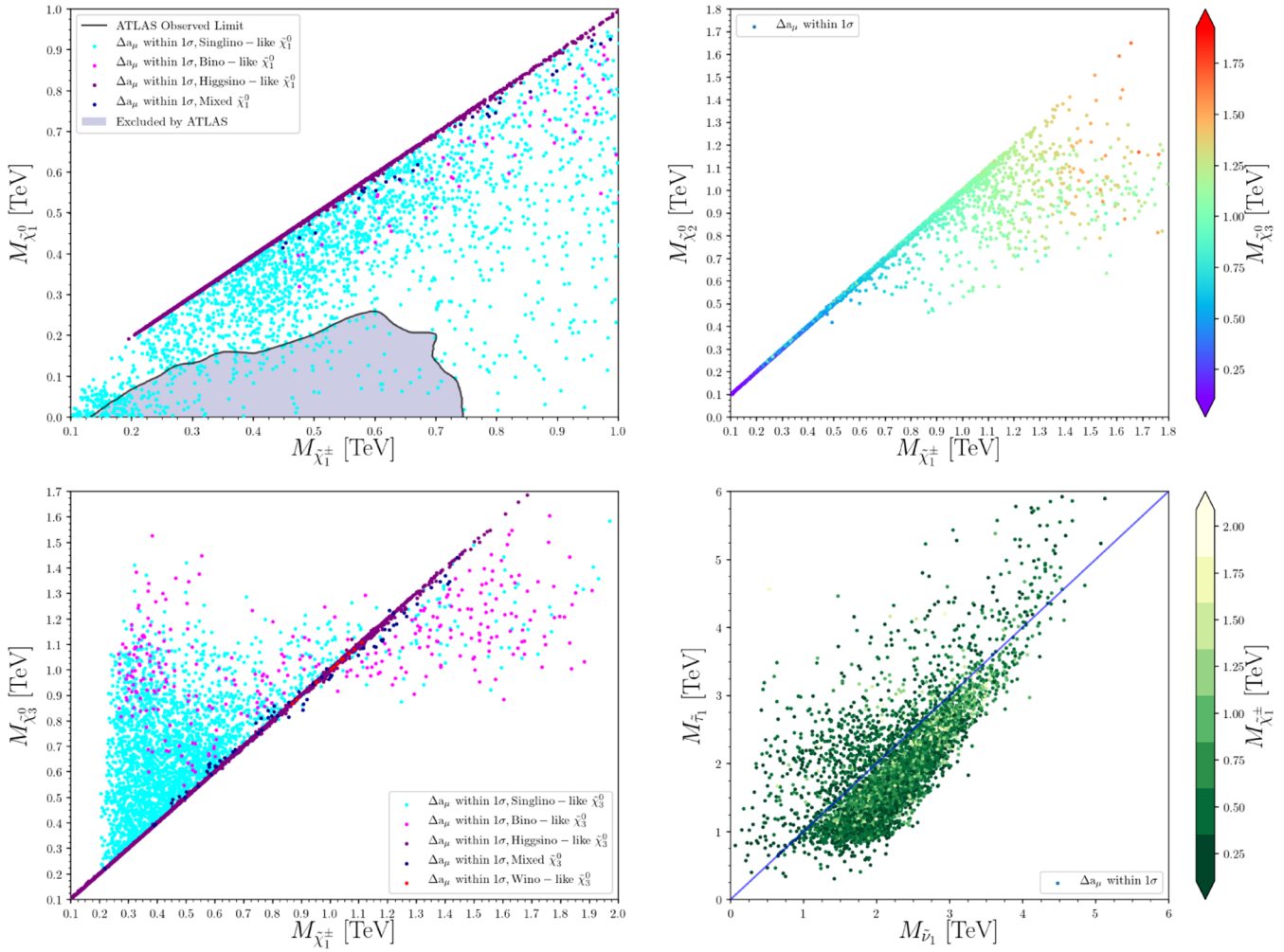

FIG. 5. Parameter regions of chargino, neutralino, (right) sneutrino, and stau masses consistent with Δa_μ within 1σ. We show the following mass mappings: (top left) lightest chargino versus lightest neutralino; (top right) lightest chargino versus second lightest neutralino; (bottom left) lightest chargino versus third lightest neutralino; (bottom right) lightest (right) sneutrino versus lightest stau. The gray region is ruled out by ATLAS searches for chargino-neutralino states [83,84]. The model solutions to the $(g-2)_\mu$ discrepancy are dominated by the neutralino (higgsinolike)-slepton and chargino-sneutrino loop contributions, where, in particular, the contributing neutralinos and charginos are light yet consistent with all experimental constraints.

$$\Delta a_e \equiv a_e^{\mathrm{exp}} - a_e^{\mathrm{SM}} = -(8.8 \pm 3.6) \times 10^{-13}.$$

The discrepancy was studied recently in the literature [98,100,101], and specifically in two-Higgs doublet models [102] and 3–3–1 models [103]. Unfortunately, in the context of our model, we cannot explain both discrepancies. The experimental observation is

$$\frac{\Delta a_e}{\Delta a_\mu} \sim (-14)\frac{m_e^2}{m_\mu^2},$$

while is known that if the BSM scenario chosen is flavor blind, as is in our case

$$\frac{\Delta a_e}{\Delta a_\mu} \sim \frac{m_e^2}{m_\mu^2}.$$

The latter is consistent with our results. A way out of this impediment would be to consider nonuniversal soft masses for smuons or selectrons. Moreover, the contributions to the electron and muon magnetic moments would have to be dominated by different diagrams with different signs. The latter would be possible if $M_1 M_2 < 0$, where M_1, M_2 are $U(1)_Y$ and $SU(2)_L$ gaugino masses, respectively, as chargino-sneutrino loops contribution is proportional to $\mathrm{sign}(\mu M_2)$ while the neutralino-slepton contribution is proportional to $\mathrm{sign}(\mu M_1)$ [104]. Our model has neither of these features. Thus, for the parameter regions consistent with Δa_μ, even at 3σ, values for Δa_e have the wrong sign

and magnitude to satisfy the discrepancy between theory and experiment.

VII. Z' SIGNAL AT COLLIDERS

In this section, we investigate the observability of a secluded UMSSM scenario with light Z' masses at LHC. To choose correct benchmarks, we first compare the range of chargino and neutralino masses with restrictions from the ATLAS searches for chargino and neutralino states [83,84]. We make use of SModelS (version 1.2.2) [105–108] in order to calculate the upper limit on the chargino-neutralino cross sections based on ATLAS-SUSY-2019-08 [83] and ATLAS-SUSY-2018-32 [84] implemented and validated with the SModelS authors. Figure 6 showcases our results in terms of the lightest chargino and neutralino masses, as functions of the ratio between our calculated cross sections versus the upper limit on the chargino-neutralino cross sections. We exclude all solutions with signal strength value exceeding 1. This plot is complementary to the one shown in the top left panel of Fig. 6, with the gray region in that plot corresponding to the area below the curve. While in the former plot, we indicate muon $g-2$ values consistent with the experiment, here, we explore neutralino and chargino masses constrained by bounds given in Table III, with the aim to choose benchmarks compatible with allowed EW-ino masses. Our plot indicates, however, that the parameter space allowed by this model is less restrictive than the one in the ATLAS analysis. We rule out some points for low chargino-neutralino masses (in red, lower left-hand corner) but allow the purple-blue points in the upper right-hand corner. The reason why we can obtain light chargino masses, without introducing new charged particles in the model is the following. The μ parameter, which affects both chargino and neutralino masses, is generated dynamically in the model and obtained by solving the renormalization group equations (RGEs). This parameter, which affects chargino and neutralino masses, is obtained using the software SPheno [45,46]. The parameter space for EW-ino masses is consistent with collider bounds from PDG [109] and the DM constraints from the previous section.

We shall concentrate our analysis in this parameter region.

Scanning over the whole range of allowed Z' mass values, we find that consistency with ATLAS production and dilepton decay results allows $M_{Z'}$ to be quite light. However, for the parameter space to satisfy both DM and muon anomalous magnetic moment constraints to at least 2σ, the Z' mass must be $M_{Z'} \gtrsim \mathcal{O}(3)$ TeV as seen from the right plane of Fig. 6. To highlight the model characteristics, we chose two benchmarks, BM I and BM II. The first benchmark is consistent with all constraints, including relic density, and satisfies the bounds on the $g-2$ factor of the muon at 1σ. The second benchmark satisfies the same constraints, except that we relax requirements on consistency with the anomalous magnetic moment of the muon. We list the values of the relevant free parameters in the model in Table IV and the corresponding mass values for the fermions and bosons in the model in Table V.

While scanning over the parameter space consistent with all constraints, we were unable to find any allowed parameter space, for which $M_{Z'} < 3.3$ TeV (BM I). Relaxing the imposed constraints on the anomalous magnetic moment of the muon completely (for BM II) while requiring agreement with the measured relic density still poses rigid constraints on the parameter space but allows a lower $M_{Z'} \sim 2.3$ TeV. The relevant predictions for BM I and BM II for the DM and $(g-2)_\mu$ observables discussed

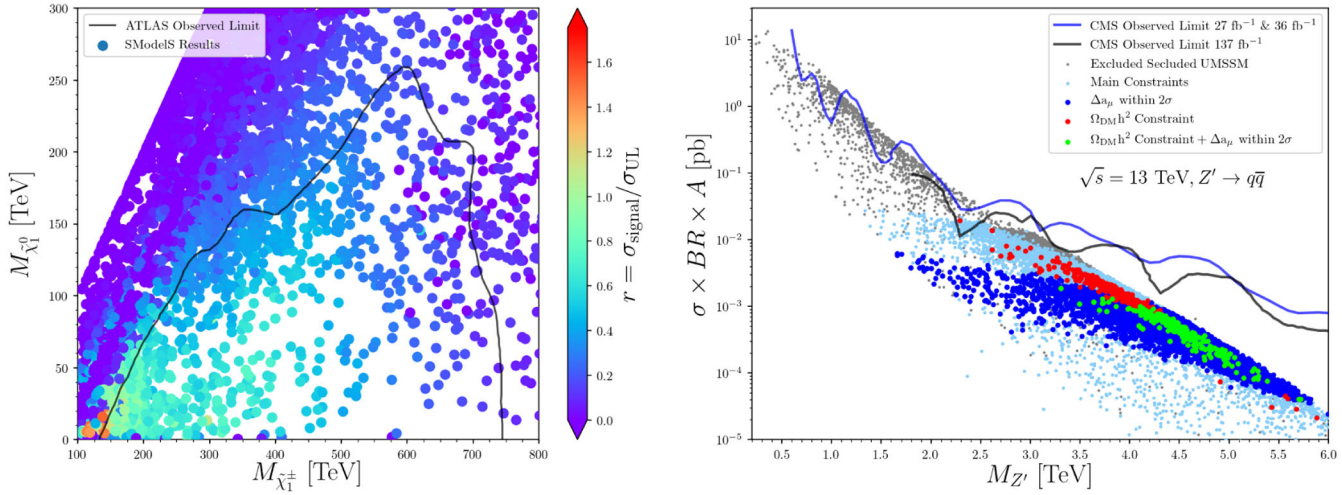

FIG. 6. (Left) Neutralino-chargino mass limits in secluded UMSSM. The black curve represents mass limits from ATLAS [83,84], while our analysis rules out only points which exceed the upper limits on the chargino-neutralino cross sections, as indicated on the right-side color bar (which gives our predicted cross section measured against the limits from ATLAS). (Right) Z' production cross sections multiplied by the dijet BRs (and by the acceptance $A = 0.5$).

TABLE IV. Set values for the free secluded UMSSM parameters, defining our benchmark scenarios BM I and BM II. Here, m_0 is the universal scalar mass, and $M_{1/2}$ the gaugino mass.

[GeV]	m_0	$M_{1/2}$	A_0	v_S	$v_{S_1} = v_{S_2} = v_{S_3}$
BM I	942	2821	662	2421	5401
BM II	1722	2568	−1092	2282	6935

	$\tan\beta$	λ	A_λ	κ	A_κ	α	δ	Y_v^{ij}
BM I	11.9	2.04×10^{-1}	3469	1.81	−4781	4.48×10^{-2}	4.44×10^{-1}	1.63×10^{-8}
BM II	20.1	9.70×10^{-2}	3051	6.73×10^{-1}	−3910	4.44×10^{-2}	4.00×10^{-1}	6.71×10^{-8}

TABLE V. Particle spectrum of BM I and BM II: bosons (top), fermions (middle), squarks, and sleptons (bottom). All masses are given in GeV.

[GeV]	$M_{Z'}$	$M_{H_1^0}$	$M_{H_2^0}$	$M_{H_3^0}$	$M_{H_4^0}$	$M_{H_5^0}$	$M_{H_6^0}$	$M_{A_1^0}$	$M_{A_2^0}$	$M_{H_1^\pm}$
BM I	3307	126	332	2559	3405	3535	4148	3405	5066	3407
BM II	2291	123	394	758	2474	3138	3332	3138	3580	3139

[GeV]	$M_{\tilde{\chi}_1^0}$	$M_{\tilde{\chi}_2^0}$	$M_{\tilde{\chi}_3^0}$	$M_{\tilde{\chi}_4^0}$	$M_{\tilde{\chi}_5^0}$	$M_{\tilde{\chi}_6^0}$	$M_{\tilde{\chi}_7^0}$	$M_{\tilde{\chi}_8^0}$	$M_{\tilde{\chi}_9^0}$	$M_{\tilde{\chi}_1^\pm}$	$M_{\tilde{\chi}_2^\pm}$	$M_{\tilde{g}}$
BM I	45	358	363	1247	2295	2321	3595	4106	4590	359	2321	5761
BM II	44	160	165	1100	1133	2122	2201	2325	3025	162	2121	5316

[GeV]	$M_{\tilde{d}_1}$	$M_{\tilde{d}_2}$	$M_{\tilde{d}_3}$	$M_{\tilde{d}_4}$	$M_{\tilde{d}_5}$	$M_{\tilde{d}_6}$	$M_{\tilde{u}_1}$	$M_{\tilde{u}_2}$	$M_{\tilde{u}_3}$	$M_{\tilde{u}_4}$	$M_{\tilde{u}_5}$	$M_{\tilde{u}_6}$
BM I	4765	4952	4989	4989	5235	5235	3896	4772	4918	4918	5234	5234
BM II	4421	4692	4817	4817	5021	5021	3499	4429	4731	4731	5021	5021

[GeV]	$M_{\tilde{\ell}_1}$	$M_{\tilde{\ell}_2}$	$M_{\tilde{\ell}_3}$	$M_{\tilde{\ell}_4}$	$M_{\tilde{\ell}_5}$	$M_{\tilde{\ell}_6}$	$M_{\tilde{\nu}_1}$	$M_{\tilde{\nu}_2}$	$M_{\tilde{\nu}_3}$	$M_{\tilde{\nu}_4}$	$M_{\tilde{\nu}_5}$	$M_{\tilde{\nu}_6}$
BM I	1333	1382	1383	2055	2071	2071	180	180	180	2053	2069	2069
BM II	1766	1912	1913	2366	2421	2422	1374	1374	1374	2364	2420	2420

in the above sections are shown in Table VI. We note that slepton masses do not necessarily need to be light to yield significant contributions to muon $g-2$. Indeed, slepton masses are mostly at TeV scale. As seen from Table IV, the lightest slepton mass is 1333 GeV for BM I and 1766 GeV for BM II. We also included the lightest slepton decays of BM I and BM II. Therefore, the current slepton searches cannot easily restrict our parameter space. We also show the stau masses in the right bottom panel of Fig. 5. As seen from the graph, the lightest stau masses are mostly $M_{\tilde{\tau}_1} > 750$ GeV. The right-sneutrino contribution is really significant for muon $g-2$ because the dominant contribution to muon $g-2$ comes from the diagram with right-sneutrinos and charginos running in the loop. This can be also seen from mass values in BM I and BM II. The light sneutrino and chargino states in BM I give significant contribution to muon $g-2$. However, the same loop effect is suppressed in the scenario BM II due to heavy sneutrino masses, and this is the reason that BM II does not contribute significantly to the muon $g-2$ as seen from Table V.

To test the signal coming from production and decay of the leptophobic Z' boson, we use its decay into supersymmetric particles, here into chargino pairs, followed by the decay into lepton pairs or jets plus missing energy.[6] The decay of the lightest chargino yielding lepton or jet final states is into $\tilde{\chi}_1^\pm \to \tilde{\chi}_1^0 W^\pm$, and we choose points for which this BR is almost 1, as shown in Table VII. In the same table, we show predictions for the LHC phenomenology of our two benchmark scenarios, including the production cross sections at a center-of-mass energy $\sqrt{s} = 13$, 14, 27, and 100 TeV, plus the dominant BRs of the Z'. For both scenarios, Z' boson production is small enough relatively to the LHC limits at a center-of-mass energy of 13 TeV. The cross section is about 0.016 fb for BM I and 0.1889 fb for BM II after accounting for the Z' boson decaying into electron and muon pairs through two chargino states.

[6]The decay into chargino pairs is not the only one yielding the required dilepton (or jets) + missing E_T signal, but it dominates other intermediate steps by a few orders of magnitude.

TABLE VI. Predictions for the BM I and BM II scenarios of the observables discussed in our dark matter analysis.

	$\Omega_{\rm DM}h^2$	$\sigma_{\rm SI}^{\rm proton}$ [pb]	$\sigma_{\rm SI}^{\rm neutron}$ [pb]	$\langle\sigma v\rangle$ [cm^3 s^{-1}]	$\Delta a_\mu \times 10^{10}$
BM I	0.131	1.84×10^{-13}	1.89×10^{-13}	5.58×10^{-29}	36.4 (within 1σ)
BM II	0.124	2.21×10^{-11}	2.26×10^{-11}	8.17×10^{-29}	173.4 (outside 3σ)

Consequently, this makes the Z' signal difficult to observe, even with more luminosity at a center-of-mass energy of 13 TeV.

The Z' can also decay into right-handed sneutrinos. Such signature has tiny SM backgrounds and would be advantageous for Z' model searches. We give, in Table VII, the BR$(Z' \to \tilde{\nu}_i^* \tilde{\nu}_i)$ for BM I and BM II where the index i can be 1, 2, and 3. As seen from the table, Z' boson of BM I decays to $\tilde{\nu}_i^* \tilde{\nu}_i$ at a rate of 3.011%. Then, each sneutrino decays to a neutrino and a neutralino LSP at a rate of 100%. This signature is not significant since the final state is nothing but only missing energy. In addition, the decay width of the lightest sneutrino is 2.18×10^{-3} GeV, and the corresponding flight time is quite short. Therefore, the sneutrino states of BM I are not long lived particles. On the other hand, the BR$(Z' \to \tilde{\nu}_i^* \tilde{\nu}_i)$ for BM II is smaller than $\mathcal{O}(<10^{-4})$.

The Z' production cross section is therefore about 0.33 fb for BM I and 3.82 fb for BM II at 13 TeV, after accounting for the Z' bosons decaying into all SM fermions (quarks + leptons) via two chargino states, giving rise to a multijet plus missing energy signature. The latter is also typically expected from supersymmetric squark and gluino production and decay so that the results of SUSY searches in the multijet plus missing energy mode could be reinterpreted to constrain the secluded UMSSM. We therefore recast these results from [110–113] with MadAnalysis 5. However, such a rate is far beyond the reach of typical multijet plus missing transverse momentum searches at the LHC, as confirmed by reinterpreting and extrapolating the results of the CMS search in [112] and the results of the ATLAS search in [110,111,113] targeting superpartner production and decay in the jets plus missing transverse momentum mode to integrated luminosity of 3 ab^{-1} with MadAnalysis 5. Consequently, this makes the Z' signal difficult to observe in dijet final states, even with more luminosity. We therefore focus on Z' signals that instead involve dileptons in the final state at a center-of-mass energy of 14 TeV and 27 TeV.

The study of [11] provides a prescription for finding leptophobic Z' bosons at the center-of-mass energy $\sqrt{s} =$ 14 TeV and 3 ab^{-1} of luminosity in the dilepton channel. The signal process consists of the resonant production of a chargino pair, followed by the decay of each chargino into a charged lepton and missing energy,

$$pp \to Z' \to \tilde{\chi}_1^\pm \tilde{\chi}_1^\mp \to \ell^+\ell^- + \not{E}_T. \tag{7.1}$$

We followed the same procedure and carried out a full Monte Carlo (MC) event simulation at the LHC, for a center-of-mass energy $\sqrt{s} = 14$ TeV and applied the cuts as in [11]. The production cross section of Z' boson is 15.8 fb for BM I and 154.4 fb for BM II for a center-of-mass energy $\sqrt{s} = 14$ TeV as given in Table VII. We have made use of FeynRules to generate a UFO [42] version of the model so that we could employ MG5a_MC@NLO (version 2.7.3) [52] for generating the hard-scattering signal event samples necessary for our collider study. These events, obtained by convoluting the hard-scattering matrix elements with the NLO set of NNPDF 3.1 parton densities [53], were subsequently matched with PYTHIA 8 (version 8.244) [114] parton showering and hadronisation algorithms, plus we simulated the typical response of an LHC detector by means of the DELPHES 3 [115] program (version 3.4.2) employing the SnowMass parameterization [116,117] that relies on the anti-k_T algorithm [118] with a radius parameter $R = 0.6$ as implemented into FastJet [119] (version 3.3.3) for event reconstruction. We have employed MadAnalysis 5 [120] (version 1.8.23) and normalized our results to an integrated luminosity of 3 ab^{-1} for the collider analysis.

TABLE VII. Z' production cross section at $\sqrt{s} = 13$, 14, 27, and 100 TeV and branching ratios for the BM I and BM II scenarios, relevant for the associated LHC phenomenology. NLO QCD corrections to the production cross sections $\sigma(pp \to Z')$ are included.

	$\sigma(pp \to Z')$ [fb]				BR$(Z' \to \tilde{\chi}_1^\pm \tilde{\chi}_1^\mp)$	BR$(Z' \to jj)$	BR$(\tilde{\chi}_1^\pm \to \tilde{\chi}_1^0 W^\pm)$
	13 TeV	14 TeV	27 TeV	100 TeV			
BM I	11.13	15.8	156.6	1942	0.059	0.309	0.99
BM II	119.7	154.4	856.2	7375	0.066	0.340	1.0

	BR$(Z' \to \tilde{\nu}_1^* \tilde{\nu}_1)$	BR$(Z' \to \tilde{\nu}_2^* \tilde{\nu}_2)$	BR$(Z' \to \tilde{\nu}_3^* \tilde{\nu}_3)$	BR$(\tilde{\nu}_{1,2,3} \to \nu_{2,1,3} \tilde{\chi}_1^0)$	BR$(\tilde{\ell}_1 \to \nu_l \tilde{\chi}_1^\pm)$
BM I	3.011×10^{-2}	3.011×10^{-2}	3.011×10^{-2}	1.0 (Each)	0.426
BM II	…	…	…	0.99 (Each)	0.237

We select events featuring two well-separated muons and veto the presence of jets by requiring

$$N^{\ell} = 2, \qquad \Delta R(\ell_1, \ell_2) > 2.5, \qquad N^{j} = 0. \tag{7.2}$$

The transverse momenta of the two leptons and the missing transverse energy are required to fulfill

$$p_T(\ell_1) > 300 \text{ GeV}, \qquad p_T(\ell_2) > 200 \text{ GeV}, \qquad \not{E}_T > 100 \text{ GeV}. \tag{7.3}$$

To investigate the observability of the two benchmarks at the HL-LHC, we use of two standard significance parameters, labeled as s and Z_A (the Asimov significance), defined as:

$$s = \frac{S}{\sqrt{B + \sigma_B^2}}, \tag{7.4}$$

$$Z_A = \sqrt{2\left((S+B)\ln\left[\frac{(S+B)(S+\sigma_B^2)}{B^2+(S+B)\sigma_B^2}\right] - \frac{B^2}{\sigma_B^2}\ln\left[1+\frac{\sigma_B^2 S}{B(B+\sigma_B^2)}\right]\right)}, \tag{7.5}$$

where S is the number of signal events, B of background events, and σ_B is the standard deviation of background events.

The corresponding cutflows are shown in Table VIII, where we give our original and final number of signal events, and the ones surviving each cut, shown in the left-handed column. We assume that we would get the same cut efficiency of the background as in [11]. Therefore, we first estimate the final number of background events (after imposing the cuts in Table VIII) at 27 TeV by using a boost factor calculated from the dominant background channel, the diboson production. We expand more on this choice. Background events at 14 TeV were generated by [116,117] and adapted from that work without regenerating them. We wanted to get an estimation about detectability of our model at the LHC. To do this, we assumed that the cut efficiency for background events would be the same when the same cuts are applied at 27 TeV instead of 14 TeV. More explicitly, [11] clearly shows that the dominant background comes from the diboson channel. Therefore, we assume that diboson production cross sections at 27 TeV divided by the diboson production cross section at 14 TeV would give us a boost factor which is found to be 2.19. Also, the number of final background events at 27 TeV, after applying all cuts, is estimated as number of final background events at 14 TeV multiplied by the boost factor, which is found to be 21.96. One can see that the significance of the benchmarks at 14 TeV and with integrated luminosity 3 ab^{-1} is very small, making it unlikely to be observed, even at the HL-LHC. Therefore, we extend the analysis of our benchmark scenarios at 27 TeV, and in Table VIII, we give our original and final number of signal events in parentheses. The significance plots, as functions of luminosity, in Fig. 7, are obtained by using the number of final background events, which is estimated as described above. While BM I remains below the 3σ minimum significance required for a positive identification, the BM II significance rises above 3σ at $\sqrt{s} = 27$ TeV and integrated luminosity 3 ab^{-1}, making this benchmark promising at the HE-LHC. That this indeed so is seen in Fig. 7, where we plot significance curves for s and Z_A at $\sqrt{s} = 27$ TeV, for both BM I and BM II, as a function of the total integrated luminosity $\mathcal{L}$. While BM I would be observable at high integrated luminosity 3 ab^{-1} at 3σ under only the most optimistic scenario, in which we assume small systematic errors ($\Delta_{\text{syst}} = 5\%$), BM II shows promise for observability even for larger systematic errors, $\Delta_{\text{syst}} = 20\%$. Of course, we stress that, while BM II is promising, it was obtained by relaxing the condition that the model satisfies $(g-2)_\mu$ to $(1\text{–}2)\sigma$.

TABLE VIII. Events surviving after each cut (as given in the left column) and significance of BM I and BM II at 14 (27) TeV and integrated luminosity 3 ab^{-1}.

Step	Requirements	BM I	BM II
0	Initial	71 (92)	726 (3854)
1	$N^{\ell} = 2$	45 (61)	386 (2310)
2	Electron Veto	13 (18)	115 (712)
3	$\lvert\eta^{\ell}\rvert < 1.5$	13 (18)	112 (685)
4	$I^{\mu}_{\text{rel}} < 0.15$	13 (18)	107 (663)
5	$\Delta R(\ell_1, \ell_2) > 2.5$	11 (18)	107 (662)
6	$N^{j} = 0$	11 (18)	60 (330)
7	$p_T(\ell_1) > 300$ GeV	6 (18)	17 (107)
8	$p_T(\ell_2) > 200$ GeV	2 (17)	6 (36)
9	$\not{E}_T > 100$ GeV	2 (15)	4 (25)
s	($\Delta_{\text{syst}} = 20\%$)	0.53 (2.33)	1.09 (3.89)
Z_A	($\Delta_{\text{syst}} = 20\%$)	0.51 (2.03)	0.99 (3.16)

For more information about the signal, we simulate the SM background events leading to final states with two charged leptons and missing energy: $t\bar{t}$, single top events, as well as single vector bosons V + jets, and dibosons VV, with V being a W boson or a Z boson decaying leptonically at 27 TeV. We include the NLO effects of the signal through a K factor. The whole QCD K factor comes from the initial state and depends on the Z'-boson mass and the set of PDFs used. Previous work provides an NLO implementation of the Z' in the $U(1)'_\chi$ model [47]. The gauge boson mass is

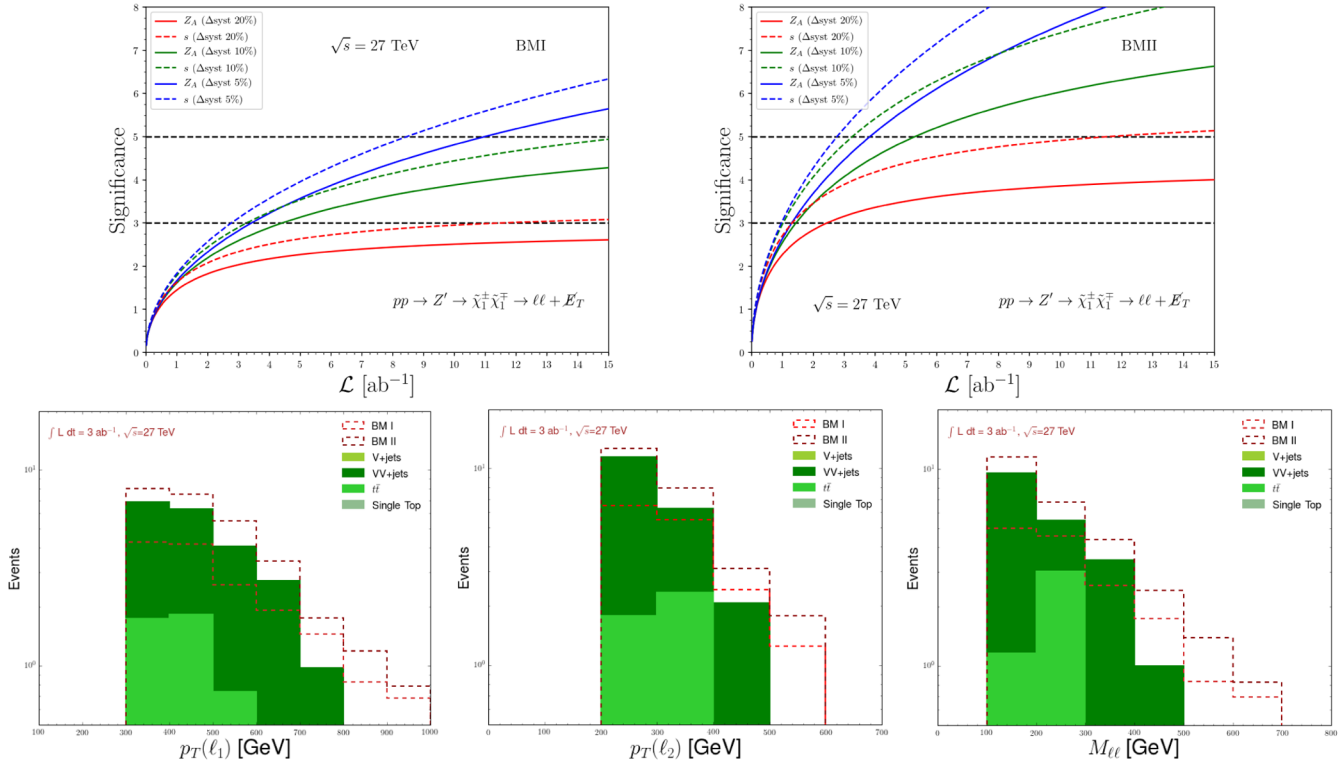

FIG. 7. Significance of benchmarks BM I (top left panel) and BM II (top right panel) at $\sqrt{s} = 27$ TeV, as a function of the luminosity $\mathcal{L}$. In each panel, we plot the usual significance s and the Asimov significance Z_A. Different curves are obtained assuming different systematic errors, as indicated in the upper left-hand panel. Bottom panels: Transverse momentum distribution of the leading muon ℓ_1 (left) and next-to-leading muon ℓ_2 (middle) and missing transverse energy spectrum (right) for BM I and BM II after applying all cuts in Table VIII. We include the SM backgrounds: $t\bar{t}$, single top, dibosons, and gauge boson + jets.

assumed to be 1 TeV, and the width is calculated to be $\Gamma_{Z'} = 12.04$ GeV, justifying a narrow width approximation. The NLO K factor for $pp \to \gamma, Z, Z' \to l^+l^-$ obtained at 1 TeV for $\sqrt{s} = 14$ TeV is 1.26.

We calculate the Z' production cross section at next-to-leading order (NLO) accuracy in QCD for $\sqrt{s} = 27$ TeV. We verified that the K factor can be inclusively calculated depending on the PDF choice and Z' mass, which enters the $Q^2 \approx M_{Z'}^2$ dependence of the PDFs. For BM I and BM II, the K factor is found to be 1.17 and 1.15, respectively. Therefore, the NLO corrections are small, and they are included in Table VII.

We include plots of the transverse momentum of the leading muon $p_T(\ell_1)$, the next-to-leading muon $p_T(\ell_2)$, and of the missing dilepton transverse energy spectrum (after applying all cuts of Table VIII) for the benchmarks in Fig. 7 and compare to the SM backgrounds. The effects of the single boson and single top are rendered negligible by the cuts imposed in Table VIII. The more promising scenario BM II is seen to rise consistently above the SM backgrounds, confirming the promise indicated in the significance plots.

VIII. SUMMARY AND CONCLUSIONS

We have presented an analysis of the secluded UMSSM, a nonminimal SUSY scenario wherein the gauge symmetry of the MSSM is augmented by a $U(1)'$ group and where a secluded sector is also added in the form of three additional scalar superfields. Their role is to separate the SUSY-breaking scale from the mass of the Z', the gauge boson introduced by the additional gauge symmetry following its spontaneous breaking, so that the latter can have a value well within the LHC reach irrespectively of the SUSY mass scale.

Our analysis here has highlighted, in particular, some novel phenomenological features pertaining to this BSM scenario, which would make it distinguishable from the MSSM or E_6 motivated UMSSM scenarios. For a start, the Z' can be leptophobic without invoking gauge kinetic mixing. Thus, one can naturally lower the experimentally imposed limits on its mass coming from its LHC hadroproduction followed by dilepton and dijet decays. In addition, and setting it apart from that of $U(1)'$ scenarios with gauge kinetic mixing, the Z' is also d-quark-phobic, allowing one to reduce its mass constraints event further.

Then, we have shown that the model predicts the existence of very light charginos and neutralinos, the lightest of the latter being a singlinolike DM candidate satisfying relic density constraints as well as direct and indirect detection bounds. In fact, alongside this new singlino state, an LSP with mass $M_{\tilde{\chi}_1^0} \lesssim 50$ GeV, our BSM scenario also accommodates a similarly light lightest chargino companion, with $M_{\tilde{\chi}_1^\pm} \lesssim 350$ GeV, both of which are respecting collider constraints. Furthermore, the next-to-LSP and next-to-next-to-LSP are higgsinos and, together with the lightest chargino, they are largely responsible (once appropriately combined with the lightest sleptons in one-loop Feynman diagrams) for obtaining a value for the muon anomalous moment consistent with experimental measurements at 1σ.

Finally, armed with such specific model setup, we have investigated the prospects of detecting such a light Z' boson in its SUSY cascade decays via the aforementioned lightest charginos and neutralinos, eventually yielding a dilepton final state in presence of significant missing transverse energy. The fact that the model is d-quark phobic, useful to reduce the mass constraints, has an adverse effect on the production cross section for Z', rendering it smaller than in the E_6 motivated UMSSM. In addition, the S, T, U parameters impose conditions on the $U(1)'$ associated charges, constraining them to be small. The secluded UMSSM is a good model for loosening Z' mass bounds, but not so promising for signal observability.

Requiring the parameter space to satisfy all experimental conditions, including the DM and $(g-2)_\mu$ ones simultaneously, or just the relic density, we have devised most favourable benchmark points with $M_{Z'} \approx 3.3$ TeV. Relaxing the $(g-2)_\mu$ requirement, our second benchmark allows $M_{Z'} \approx 2.3$ TeV. Of the two benchmarks, the latter one shows more promise to be observed at the HE-LHC at 3σ or better, as proved from a prototypical MC analysis performed, while the former would be observed only assuming small systematic errors. Our analysis should justify dedicated searches with real data from ATLAS and/or CMS. In summary, we enumerate the interesting and novel features of our model:

(i) The model framework is not new but ours is the only up-to-date study of its phenomenology.
(ii) The conditions for gauge invariance and anomaly cancellations have appeared before. There are linear, quadratic, and cubic in the $U(1)'$ charges, and they also depend on the electric charges and number of generations of the exotic fermions. Solving them is nontrivial and finding a solution obeying rational numbers for exotic fermion charges requirements even less so.
(iii) Our choice of $U(1)'$ charges is innovative because it renders this to be a $U(1)'$ model, which is leptophobic *without* kinetic mixing, or requiring family-non-universality. Our choice of $U(1)'$ charges, which affects this, is particularly simple and transparent.
(iv) The model was previously used because it decouples the Z' scale from the SUSY sector: Z' was always considered to be heavy, while the chargino-neutralino sector could be light. In our scenario, both charginos and neutralinos can be light; at the same time Z', since it is leptohobic, can also be light. A model featuring *both* a very light singlino <50 GeV (escaping LHC bounds) *and* a light Z', while obeying family universality, is new.
(v) While a light singlino is possible in secluded models (containing extra singlet fields), here, we implement it in the context of a leptophobic scenario.
(vi) In addition, we have shown that we can distinguish this scenario from E_6 motivated $U(1)'$ models with kinetic mixing, because in our scenario, the Z' is d-quark phobic. Again, this is a novel feature in universal Z' models.
(vii) In this model, we have also investigated and found out a link between satisfying $(g-2)_\mu$ and relaxing mass constraints on Z'.
(viii) Finally, the model can be tested at the HL-LHC, making it relevant for searches at Run III.

ACKNOWLEDGMENTS

Parts of the numerical calculations reported in this paper were performed using High Performance Computing (HPC), managed by Calcul Québec and Compute Canada, and the IRIDIS High Performance Computing Facility, and associated support services, at the University of Southampton. The database entry for ATLAS-SUSY-2019-08 and ATLAS-SUSY-2018-32 were implemented and validated by the SModelS authors upon request, for which we are grateful to Sabine Kraml and Wolfgang Waltenberger. S. M. is supported, in part, through the NExT Institute and the STFC consolidated Grant No. ST/L000296/1. The work of M. F. and Ö. Ö. has been partly supported by NSERC through Grant No. SAP105354, and by MITACS International Fellowship. The work of Y. H. is supported by The Scientific and Technological Research Council of Turkey (TUBITAK) in the framework of the 2219-International Postdoctoral Research Fellowship program, and by Balikesir University Scientific Research Projects with Grant No. BAP-2017/198.

APPENDIX: ANOMALY CANCELLATION CONDITIONS

Partial anomaly conditions have been explored before in [33], and complete expressions exist in [26]. As our choices for $U(1)'$ differ from the usual assignments, we include them here, for completeness. For the model to be anomaly free, the $U(1)'$ charges of fields must satisfy,

$$0 = 3(2Q_Q + Q_U + Q_D) + n_\Upsilon(Q_\Upsilon + Q_{\bar{\Upsilon}}), \quad \text{(A1)}$$

$$0 = 3(3Q_Q + Q_L) + Q_{H_d} + Q_{H_u}, \quad \text{(A2)}$$

$$0 = 3\left(\frac{1}{6}Q_Q + \frac{1}{3}Q_D + \frac{4}{3}Q_U + \frac{1}{2}Q_L + Q_E\right) + \frac{1}{2}(Q_{H_d} + Q_{H_u}) + 3n_\Upsilon Y_\Upsilon^2(Q_\Upsilon + Q_{\bar{\Upsilon}}) + n_\varphi Y_\varphi^2(Q_\varphi + Q_{\bar{\varphi}}), \quad \text{(A3)}$$

$$0 = 3(6Q_Q + 3Q_U + 3Q_D + 2Q_\ell + Q_e + Q_N) + 2Q_{H_d} + 2Q_{H_u} + Q_S + Q_{S_1} + Q_{S_2} + Q_{S_3} + 3n_\Upsilon(Q_\Upsilon + Q_{\bar{\Upsilon}}) + n_\varphi(Q_\varphi + Q_{\bar{\varphi}}), \quad \text{(A4)}$$

$$0 = 3(Q_Q^2 + Q_D^2 - 2Q_U^2 - Q_\ell^2 + Q_e^2) - Q_{H_d}^2 + Q_{H_u}^2 + 3n_\Upsilon Y_\Upsilon(Q_\Upsilon^2 - Q_{\bar{\Upsilon}}^2) + n_\varphi Y_\varphi(Q_\varphi^2 - Q_{\bar{\varphi}}^2), \quad \text{(A5)}$$

$$0 = 3(6Q_Q^3 + 3Q_D^3 + 3Q_U^3 + 2Q_\ell^3 + Q_e^3 + Q_N^3) + 2Q_{H_d}^3 + 2Q_{H_u}^3 + Q_S^3 + Q_{S_1}^3 + Q_{S_2}^3 + Q_{S_3}^3 + 3n_\Upsilon(Q_\Upsilon^3 + Q_{\bar{\Upsilon}}^3) + n_\varphi(Q_\varphi^3 + Q_{\bar{\varphi}}^3), \quad \text{(A6)}$$

which correspond to vanishing of $U(1)'$-$SU(3)_C$-$SU(3)_C$, $U(1)'$-$SU(2)_L$-$SU(2)_L$, $U(1)'$-$U(1)_Y$-$U(1)_Y$, $U(1)'$-graviton-graviton, $U(1)'$-$U(1)'$-$U(1)_Y$, and $U(1)'$-$U(1)'$-$U(1)'$ anomalies, respectively. All these anomaly cancellation conditions are satisfied for a particular pattern of charges and parameters. The $U(1)'$ charges for Higgs fields in the model are chosen as

$$Q_{S_2} = -2Q_{S_1} = -2Q_{S_3}, \qquad Q_{H_u} + Q_{H_d} + Q_S = 0. \quad \text{(A7)}$$

For the $U(1)$ charge assignments in the model, [Eq. (2.7)], the exotic fields satisfy the relations,

$$\begin{aligned} n_\Upsilon[Q_\Upsilon + Q_{\bar{\Upsilon}}] &= -27\alpha \\ n_\varphi[Q_\varphi + Q_{\bar{\varphi}}] &= -18\alpha \\ 9Y_\Upsilon^2 + 2Y_\varphi^2 &= 9 \\ 9Y_\Upsilon[Q_\Upsilon - Q_{\bar{\Upsilon}}] + 2Y_\varphi[Q_\varphi - Q_{\bar{\varphi}}] &= 33\alpha \\ 3n_\Upsilon[Q_\Upsilon^3 + Q_{\bar{\Upsilon}}^3] + n_\varphi[Q_\varphi^3 + Q_{\bar{\varphi}}^3] &= 6(\delta^3 - 999\alpha^3). \end{aligned} \quad \text{(A8)}$$

We found that a possible solution to the mixed anomaly constraints allows $n_\Upsilon = 3$ color-triplet pairs with hypercharge $Y_\Upsilon = \pm 1/3$ and $n_\varphi = 2$ singlet pairs with $Y_\varphi = \pm 2$. This still allows some freedom in the $U(1)'$ charges of Υ, $\bar{\Upsilon}$, and φ, $\bar{\varphi}$ as solutions of the last quartic equations.

[1] M. Cvetic and P. Langacker, New gauge bosons from string models, Mod. Phys. Lett. A **11**, 1247 (1996).

[2] D. Suematsu and Y. Yamagishi, Radiative symmetry breaking in a supersymmetric model with an extra U(1), Int. J. Mod. Phys. A **10**, 4521 (1995).

[3] H.-S. Lee, K. T. Matchev, and T. T. Wang, A U(1) -prime solution to the μ^- problem and the proton decay problem in supersymmetry without R-parity, Phys. Rev. D **77**, 015016 (2008).

[4] D. A. Demir, Two Higgs doublet models from TeV scale supersymmetric extra U(1) models, Phys. Rev. D **59**, 015002 (1998).

[5] D. A. Demir and Y. Farzan, Correlating mu parameter and right-handed neutrino masses in $N = 1$ supergravity, J. High Energy Phys. 03 (2006) 010.

[6] D. A. Demir, L. L. Everett, and P. Langacker, Dirac Neutrino Masses from Generalized Supersymmetry Breaking, Phys. Rev. Lett. **100**, 091804 (2008).

[7] P. Langacker, The physics of heavy Z' gauge bosons, Rev. Mod. Phys. **81**, 1199 (2009).

[8] J. Erler, P. Langacker, S. Munir, and E. Rojas, Improved constraints on Z-prime bosons from electroweak precision data, J. High Energy Phys. 08 (2009) 017.

[9] O. C. Anoka, K. S. Babu, and I. Gogoladze, Constraining Z-prime from supersymmetry breaking, Nucl. Phys. **B687**, 3 (2004).

[10] G. Aad *et al.* (ATLAS Collaboration), Search for high-mass dilepton resonances using 139 fb^{-1} of pp collision data collected at $\sqrt{s} = 13$ TeV with the ATLAS detector, Phys. Lett. B **796**, 68 (2019).

[11] J. Y. Araz, G. Corcella, M. Frank, and B. Fuks, Loopholes in Z' searches at the LHC: Exploring supersymmetric and leptophobic scenarios, J. High Energy Phys. 02 (2018) 092.

[12] A. M. Sirunyan *et al.* (CMS Collaboration), Search for high mass dijet resonances with a new background

prediction method in proton-proton collisions at $\sqrt{s} = 13$ TeV, J. High Energy Phys. 05 (2020) 033.
[13] B. Coleppa, S. Kumar, and A. Sarkar, Fermiophobic gauge boson phenomenology in 221 Models, Phys. Rev. D **98**, 095009 (2018).
[14] T. G. Rizzo, Gauge kinetic mixing and leptophobic Z' in E(6) and SO(10), Phys. Rev. D **59**, 015020 (1998).
[15] K. S. Babu, C. F. Kolda, and J. March-Russell, Leptophobic U(1) s and the R(b)-R(c) crisis, Phys. Rev. D **54**, 4635 (1996).
[16] C.-W. Chiang, T. Nomura, and K. Yagyu, Phenomenology of E_6-inspired leptophobic Z' boson at the LHC, J. High Energy Phys. 05 (2014) 106.
[17] A. Celis, J. Fuentes-Martin, M. Jung, and H. Serodio, Family nonuniversal Z' models with protected flavor-changing interactions, Phys. Rev. D **92**, 015007 (2015).
[18] B. Allanach, J. Butterworth, and T. Corbett, Collider constraints on Z' models for neutral current B-anomalies, J. High Energy Phys. 08 (2019) 106.
[19] J. Alvarado, C. E. Diaz, and R. Martinez, A $U(1)_X$ extension to the MSSM with three families, in *Meeting of the Division of particles and Fields of the American Physical Society, 2019*, Vol. 9.
[20] S. Mantilla, R. Martinez, and F. Ochoa, Neutrino and *CP*-even Higgs boson masses in a nonuniversal U$(1)'$ extension, Phys. Rev. D **95**, 095037 (2017).
[21] Y. Tang and Y.-L. Wu, Flavor non-universal gauge interactions and anomalies in B-meson decays, Chin. Phys. C **42**, 033104 (2018).
[22] J. F. Kamenik, Y. Soreq, and J. Zupan, Lepton flavor universality violation without new sources of quark flavor violation, Phys. Rev. D **97**, 035002 (2018).
[23] A. Alves, S. Profumo, and F. S. Queiroz, The dark Z' portal: Direct, indirect and collider searches, J. High Energy Phys. 04 (2014) 063.
[24] J. Erler, P. Langacker, and T.-j. Li, The Z-Z' mass hierarchy in a supersymmetric model with a secluded U(1) -prime breaking sector, Phys. Rev. D **66**, 015002 (2002).
[25] C.-W. Chiang and E. Senaha, Electroweak phase transitions in the secluded U(1)-prime-extended MSSM, J. High Energy Phys. 06 (2010) 030.
[26] D. A. Demir, M. Frank, L. Selbuz, and I. Turan, Scalar neutrinos at the LHC, Phys. Rev. D **83**, 095001 (2011).
[27] J. Kang, P. Langacker, and B. D. Nelson, Theory and phenomenology of exotic isosinglet quarks and squarks, Phys. Rev. D **77**, 035003 (2008).
[28] M. Frank, L. Selbuz, and I. Turan, Neutralino and chargino production in U(1)' at the LHC, Eur. Phys. J. C **73**, 2656 (2013).
[29] P. Langacker and J. Wang, U(1)-prime symmetry breaking in supersymmetric E(6) models, Phys. Rev. D **58**, 115010 (1998).
[30] J. Kang and P. Langacker, Z' discovery limits for supersymmetric E(6) models, Phys. Rev. D **71**, 035014 (2005).
[31] J. L. Hewett and T. G. Rizzo, Low-energy phenomenology of superstring inspired E(6) models, Phys. Rep. **183**, 193 (1989).
[32] P. Langacker, Grand unified theories and proton decay, Phys. Rep. **72**, 185 (1981).
[33] J. Kang, P. Langacker, T.-j. Li, and T. Liu, Electroweak Baryogenesis in a Supersymmetric U(1)-Prime Model, Phys. Rev. Lett. **94**, 061801 (2005).
[34] V. Barger, P. Langacker, and H.-S. Lee, Big bang nucleosynthesis constraints on Z' properties, in *11th International Conference on Supersymmetry and the Unification of Fundamental Interactions, 2004*, Vol. 2.
[35] M. Kazana *et al.* (ATLAS and CMS Collaborations), Searches for heavy stable charged particles and other exotic signatures with large ionization at the LHC, CMS-CR-2016-003, 132 (2016).
[36] J. L. Rosner, Mixing of charge $-1/3$ quarks and charged leptons with exotic fermions in E(6), arXiv:hep-ph/9907438.
[37] M. Frank, Y. Hiçyılmaz, S. Moretti, and Ö. Özdal, E_6 motivated UMSSM confronts experimental data, J. High Energy Phys. 05 (2020) 123.
[38] F. Staub, SARAH, arXiv:0806.0538.
[39] F. Staub, Automatic calculation of supersymmetric renormalization group equations and self energies, Comput. Phys. Commun. **182**, 808 (2011).
[40] F. Staub, Exploring new models in all detail with SARAH, Adv. High Energy Phys. **2015**, 840780 (2015).
[41] A. Belyaev, N. D. Christensen, and A. Pukhov, CalcHep 3.4 for collider physics within and beyond the Standard Model, Comput. Phys. Commun. **184**, 1729 (2013).
[42] C. Degrande, C. Duhr, B. Fuks, D. Grellscheid, O. Mattelaer, and T. Reiter, UFO—The Universal FeynRules output, Comput. Phys. Commun. **183**, 1201 (2012).
[43] N. D. Christensen, P. de Aquino, C. Degrande, C. Duhr, B. Fuks, M. Herquet, F. Maltoni, and S. Schumann, A comprehensive approach to new physics simulations, Eur. Phys. J. C **71**, 1541 (2011).
[44] G. Bélanger, F. Boudjema, A. Goudelis, A. Pukhov, and B. Zaldivar, MicrOMEGAs5.0: Freeze-in, Comput. Phys. Commun. **231**, 173 (2018).
[45] W. Porod, SPheno, a program for calculating supersymmetric spectra, SUSY particle decays and SUSY particle production at e+ e- colliders, Comput. Phys. Commun. **153**, 275 (2003).
[46] W. Porod and F. Staub, SPheno 3.1: Extensions including flavour, *CP*-phases and models beyond the MSSM, Comput. Phys. Commun. **183**, 2458 (2012).
[47] B. Fuks, M. Klasen, F. Ledroit, Q. Li, and J. Morel, Precision predictions for Z'-production at the CERN LHC: QCD matrix elements, parton showers, and joint resummation, Nucl. Phys. **B797**, 322 (2008).
[48] B. Fuks and R. Ruiz, A comprehensive framework for studying W' and Z' bosons at hadron colliders with automated jet veto resummation, J. High Energy Phys. 05 (2017) 032.
[49] A. Alloul, N. D. Christensen, C. Degrande, C. Duhr, and B. Fuks, FeynRules 2.0—A complete toolbox for tree-level phenomenology, Comput. Phys. Commun. **185**, 2250 (2014).
[50] C. Degrande, Automatic evaluation of UV and R2 terms for beyond the Standard Model Lagrangians: A proof-of-principle, Comput. Phys. Commun. **197**, 239 (2015).
[51] T. Hahn, Generating Feynman diagrams and amplitudes with FeynArts 3, Comput. Phys. Commun. **140**, 418 (2001).

[52] J. Alwall, R. Frederix, S. Frixione, V. Hirschi, F. Maltoni, O. Mattelaer, H.-S. Shao, T. Stelzer, P. Torrielli, and M. Zaro, The automated computation of tree-level and next-to-leading order differential cross sections, and their matching to parton shower simulations, J. High Energy Phys. 07 (2014) 079.
[53] R. D. Ball *et al.* (NNPDF Collaboration), Parton distributions from high-precision collider data, Eur. Phys. J. C **77**, 663 (2017).
[54] A. M. Sirunyan *et al.* (CMS Collaboration), Search for narrow and broad dijet resonances in proton-proton collisions at $\sqrt{s} = 13$ TeV and constraints on dark matter mediators and other new particles, J. High Energy Phys. 08 (2018) 130.
[55] P. Bechtle, O. Brein, S. Heinemeyer, O. Stål, T. Stefaniak, G. Weiglein, and K. E. Williams, HiggsBounds – 4: Improved Tests of Extended Higgs Sectors against exclusion Bounds from LEP, the Tevatron and the LHC, Eur. Phys. J. C **74**, 2693 (2014).
[56] P. Bechtle, S. Heinemeyer, O. Stål, T. Stefaniak, and G. Weiglein, HiggsSignals: Confronting arbitrary Higgs sectors with measurements at the Tevatron and the LHC, Eur. Phys. J. C **74**, 2711 (2014).
[57] A. Buckley, PySLHA: A pythonic interface to SUSY Les Houches Accord data, Eur. Phys. J. C **75**, 467 (2015).
[58] P. Z. Skands *et al.*, SUSY Les Houches accord: Interfacing SUSY spectrum calculators, decay packages, and event generators, J. High Energy Phys. 07 (2004) 036.
[59] G. Cacciapaglia, C. Csaki, G. Marandella, and A. Strumia, The minimal set of electroweak precision parameters, Phys. Rev. D **74**, 033011 (2006).
[60] G. Altarelli and R. Barbieri, Vacuum polarization effects of new physics on electroweak processes, Phys. Lett. B **253**, 161 (1991).
[61] M. E. Peskin and T. Takeuchi, A New Constraint on a Strongly Interacting Higgs Sector, Phys. Rev. Lett. **65**, 964 (1990).
[62] M. E. Peskin and T. Takeuchi, Estimation of oblique electroweak corrections, Phys. Rev. D **46**, 381 (1992).
[63] I. Maksymyk, C. P. Burgess, and D. London, Beyond S, T and U, Phys. Rev. D **50**, 529 (1994).
[64] M. Baak, J. Cúth, J. Haller, A. Hoecker, R. Kogler, K. Mönig, M. Schott, and J. Stelzer (Gfitter Group Collaboration), The global electroweak fit at NNLO and prospects for the LHC and ILC, Eur. Phys. J. C **74**, 3046 (2014).
[65] M. Tanabashi *et al.* (particle Data GroupCollaboration), Review of particle physics, Phys. Rev. D **98**, 030001 (2018).
[66] S. Chatrchyan *et al.* (CMS Collaboration), Observation of a new boson at a mass of 125 GeV with the CMS experiment at the LHC, Phys. Lett. B **716**, 30 (2012).
[67] R. Aaij *et al.* (LHCb Collaboration), First Evidence for the Decay $B_s^0 \to \mu^+\mu^-$, Phys. Rev. Lett. **110**, 021801 (2013).
[68] D. Asner *et al.* (Heavy Flavor Averaging Group Collaboration), Averages of b-hadron, c-hadron, and τ-lepton properties, arXiv:1010.1589.
[69] Y. Amhis *et al.* (Heavy Flavor Averaging Group Collaboration), Averages of B-hadron, C-hadron, and tau-lepton properties as of early 2012, arXiv:1207.1158.
[70] H. Bahl, S. Heinemeyer, W. Hollik, and G. Weiglein, Theoretical uncertainties in the MSSM Higgs boson mass calculation, Eur. Phys. J. C **80**, 497 (2020).
[71] I. Gogoladze, R. Khalid, S. Raza, and Q. Shafi, Higgs and Sparticle spectroscopy with Gauge-Yukawa unification, J. High Energy Phys. 06 (2011) 117.
[72] I. Gogoladze, Q. Shafi, and C. S. Un, Higgs boson mass from t-b-τ Yukawa unification, J. High Energy Phys. 08 (2012) 028.
[73] M. A. Ajaib, I. Gogoladze, Q. Shafi, and C. S. Un, A predictive Yukawa unified SO(10) model: Higgs and Sparticle masses, J. High Energy Phys. 07 (2013) 139.
[74] C. S. Un and Ö. Özdal, Mass spectrum and Higgs profile in BLSSM, Phys. Rev. D **93**, 055024 (2016).
[75] P. A. R. Ade *et al.* (Planck Collaboration), Planck 2013 results. XVI. Cosmological parameters, Astron. Astrophys. **571**, A16 (2014).
[76] N. Aghanim *et al.* (Planck Collaboration), Planck 2018 results. VI. Cosmological parameters, Astron. Astrophys. **641**, A6 (2020).
[77] N. Arkani-Hamed, A. Delgado, and G. Giudice, The Well-tempered neutralino, Nucl. Phys. **B741**, 108 (2006).
[78] J. Cao, Y. He, L. Shang, W. Su, and Y. Zhang, Testing the light dark matter scenario of the MSSM at the LHC, J. High Energy Phys. 03 (2016) 207.
[79] L. Calibbi, J. M. Lindert, T. Ota, and Y. Takanishi, Cornering light neutralino dark matter at the LHC, J. High Energy Phys. 10 (2013) 132.
[80] U. Ellwanger, Present status and future tests of the Higgsino-Singlino sector in the NMSSM, J. High Energy Phys. 02 (2017) 051.
[81] G. Bélanger, J. Da Silva, U. Laa, and A. Pukhov, Probing U(1) extensions of the MSSM at the LHC Run I and in dark matter searches, J. High Energy Phys. 09 (2015) 151.
[82] V. Barger, C. Kao, P. Langacker, and H.-S. Lee, Neutralino relic density in a supersymmetric U(1)-prime model, Phys. Lett. B **600**, 104 (2004).
[83] G. Aad *et al.* (ATLAS Collaboration), Search for direct production of electroweakinos in final states with one lepton, missing transverse momentum and a Higgs boson decaying into two b-jets in (pp) collisions at $\sqrt{s} = 13$ TeV with the ATLAS detector, Eur. Phys. J. C **80**, 691 (2020).
[84] G. Aad *et al.* (ATLAS Collaboration), Search for electroweak production of charginos and sleptons decaying into final states with two leptons and missing transverse momentum in $\sqrt{s} = 13$ TeV pp collisions using the ATLAS detector, Eur. Phys. J. C **80**, 123 (2020).
[85] M. Frank and Ö. Özdal, Exploring the supersymmetric $\mathrm{U}(1)_{B-L} \times \mathrm{U}(1)_R$ model with dark matter, muon $g-2$ and Z' mass limits, Phys. Rev. D **97**, 015012 (2018).
[86] J. Y. Araz, M. Frank, and B. Fuks, Differentiating $U(1)'$ supersymmetric models with right sneutrino and neutralino dark matter, Phys. Rev. D **96**, 015017 (2017).
[87] E. Aprile *et al.* (XENON Collaboration), Dark Matter Search Results from a One Ton-Year Exposure of Xenon1t, Phys. Rev. Lett. **121**, 111302 (2018).
[88] J. Aalbers *et al.* (DARWIN Collaboration), DARWIN: Towards the ultimate dark matter detector, J. Cosmol. Astropart. Phys. 11 (2016) 017.

[89] M. Ackermann *et al.* (Fermi-LAT Collaboration), Searching for Dark Matter Annihilation from Milky Way Dwarf Spheroidal Galaxies with Six Years of Fermi Large Area Telescope Data, Phys. Rev. Lett. **115**, 231301 (2015).

[90] M. L. Ahnen *et al.* (MAGIC and Fermi-LAT Collaboration), Limits to dark matter annihilation cross-section from a combined analysis of MAGIC and Fermi-LAT observations of Dwarf satellite galaxies, J. Cosmol. Astropart. Phys. 02 (2016) 039.

[91] G. W. Bennett *et al.* (Muon g-2 Collaboration), Final report of the muon E821 anomalous magnetic moment measurement at BNL, Phys. Rev. D **73**, 072003 (2006).

[92] R. H. Parker, C. Yu, W. Zhong, B. Estey, and H. Muller, Measurement of the fine-structure constant as a test of the standard model, Science **360**, 191 (2018).

[93] A. M. Sirunyan *et al.* (CMS Collaboration), Search for supersymmetry in proton-proton collisions at 13 TeV in final states with jets and missing transverse momentum, J. High Energy Phys. 10 (2019) 244.

[94] A. M. Sirunyan *et al.* (CMS Collaboration), Search for supersymmetric partners of electrons and muons in proton-proton collisions at $\sqrt{s} = 13$ TeV, Phys. Lett. B **790**, 140 (2019).

[95] A. M. Sirunyan *et al.* (CMS Collaboration), Search for Supersymmetry with a Compressed Mass Spectrum in Events with a Soft τ Lepton, a Highly Energetic Jet, and Large Missing Transverse Momentum in Proton-Proton Collisions at $\sqrt{s} =$ TeV, Phys. Rev. Lett. **124**, 041803 (2020).

[96] ATLAS Collaboration, Search for direct stau production in events with two hadronic tau leptons in $\sqrt{s} = 13$ TeV pp collisions with the ATLAS detector.

[97] T. Aoyama, M. Hayakawa, T. Kinoshita, and M. Nio, Tenth-order electron anomalous magnetic moment—Contribution of diagrams without closed lepton loops, Phys. Rev. D **91**, 033006 (2015); Erratum: Phys. Rev. D **96**, 019901 (2017).

[98] S. Volkov, Numerical calculation of high-order QED contributions to the electron anomalous magnetic moment, Phys. Rev. D **98**, 076018 (2018).

[99] T. Aoyama, T. Kinoshita, and M. Nio, Revised and improved value of the QED tenth-order electron anomalous magnetic moment, Phys. Rev. D **97**, 036001 (2018).

[100] S. Volkov, New method of computing the contributions of graphs without lepton loops to the electron anomalous magnetic moment in QED, Phys. Rev. D **96**, 096018 (2017).

[101] T. Aoyama, T. Kinoshita, and M. Nio, Theory of the anomalous magnetic moment of the electron, Atoms **7**, 28 (2019).

[102] E. J. Chun, J. Kim, and T. Mondal, Electron EDM and muon anomalous magnetic moment in two-Higgs-doublet models, J. High Energy Phys. 12 (2019) 068.

[103] G. De Conto and V. Pleitez, Electron and muon anomalous magnetic dipole moment in a 3–3–1 model, J. High Energy Phys. 05 (2017) 104.

[104] M. Badziak and K. Sakurai, Explanation of electron and muon $g-2$ anomalies in the MSSM, J. High Energy Phys. 10 (2019) 024.

[105] F. Ambrogi, S. Kraml, S. Kulkarni, U. Laa, A. Lessa, V. Magerl, J. Sonneveld, M. Traub, and W. Waltenberger, SModelS v1.1 user manual: Improving simplified model constraints with efficiency maps, Comput. Phys. Commun. **227**, 72 (2018).

[106] F. Ambrogi *et al.*, SModelS v1.2: Long-lived particles, combination of signal regions, and other novelties, Comput. Phys. Commun. **251**, 106848 (2020).

[107] J. Dutta, S. Kraml, A. Lessa, and W. Waltenberger, SModelS extension with the CMS supersymmetry search results from Run 2, Lett. High Energy Phys. **1**, 5 (2018).

[108] C. K. Khosa, S. Kraml, A. Lessa, P. Neuhuber, and W. Waltenberger, SModelS database update v1.2.3, Lett. High Energy Phys. **158**, 2020 (2020).

[109] P. Zyla *et al.* (particle Data Group Collaboration), Review of particle physics, Prog. Theor. Exp. Phys. **2020**, 083C01 (2020).

[110] M. Aaboud *et al.* (ATLAS Collaboration), Search for squarks and gluinos in final states with jets and missing transverse momentum at $\sqrt{s} = 13$ TeV with the ATLAS detector, Eur. Phys. J. C **76**, 392 (2016).

[111] M. Aaboud *et al.* (ATLAS Collaboration), Search for squarks and gluinos in final states with jets and missing transverse momentum using 36 fb^{-1} of $\sqrt{s} = 13$ TeV pp collision data with the ATLAS detector, Phys. Rev. D **97**, 112001 (2018).

[112] A. M. Sirunyan *et al.* (CMS Collaboration), Search for supersymmetry in multijet events with missing transverse momentum in proton-proton collisions at 13 TeV, Phys. Rev. D **96**, 032003 (2017).

[113] ATLAS Collaboration, Search for squarks and gluinos in final states with jets and missing transverse momentum using 139 fb^{-1} of $\sqrt{s} = 13$ TeV pp collision data with the ATLAS detector.

[114] T. Sjöstrand, S. Ask, J. R. Christiansen, R. Corke, N. Desai, P. Ilten, S. Mrenna, S. Prestel, C. O. Rasmussen, and P. Z. Skands, An introduction to PYTHIA 8.2, Comput. Phys. Commun. **191**, 159 (2015).

[115] J. de Favereau, C. Delaere, P. Demin, A. Giammanco, V. Lemaître, A. Mertens, and M. Selvaggi (DELPHES 3 Collaboration), DELPHES 3, A modular framework for fast simulation of a generic collider experiment, J. High Energy Phys. 02 (2014) 057.

[116] J. Anderson *et al.*, SnowMass energy frontier simulations, arxiv:1309.1057.

[117] A. Avetisyan *et al.*, Methods and results for Standard Model event generation at $\sqrt{s} = 14$ TeV, 33 TeV and 100 TeV proton colliders (a snowmass whitepaper), in Community Summer Study 2013: SnowMass on the Mississippi, 8, 2013, http://arxiv.org/abs/1308.1636.

[118] M. Cacciari, G. P. Salam, and G. Soyez, The anti-k_t jet clustering algorithm, J. High Energy Phys. 04 (2008) 063.

[119] M. Cacciari, G. P. Salam, and G. Soyez, FastJet user manual, Eur. Phys. J. C **72**, 1896 (2012).

[120] E. Conte, B. Fuks, and G. Serret, MadAnalysis 5, a user-friendly framework for collider phenomenology, Comput. Phys. Commun. **184**, 222 (2013).